Characterization of variability of Total Electron Content (TEC) over Malindi

By

George Ochieng Ondede

A Thesis Submitted in Partial Fulfillment of the Requirements for the Degree of Masters of Science in Physics

The Department of Physics and Material Science

Maseno University

Abstract

The dynamics of the ionosphere depends largely on solar activity. The attenuation of radio signals as they propagate through the ionosphere can be determined through a parameter called the Total Electron Content (TEC), which is a measure of the number of electrons along a line of sight. The variability of TEC is critical around the dip equatorial region especially within 15^0 North and South where we experience anomalously enhanced TEC in the ionosphere. This study focused on the characterization of the variability of TEC over Malindi, Kenya (03.03°N, 40.13°E), and the variability studies were carried out using inter-quartile range as the parameter, with goal of coming up with a morphological description of TEC that would be useful in the understanding of the space weather conditions over Kenya. The objectives of the study were to obtain plots of TEC against time for each day of the four months, January, April, July and October, representing four seasons, of the years 1999, 2000, 2001 and 2002 and to characterize the variability of the TEC during the period of study. The diurnal variability was greatest during the early morning and late evening hours of the local time and minimum during the midday and midnight. The seasonal variability was greatest during the March equinox, moderate during the summer equinox and least during the solstices. There was observed enhanced night-time variability just before midnight, which could be attributed to neutral winds. Of the four years studied, 2000 and 2001 experienced the highest level of TEC variability and a TEC variability level of between 12 and 30 TECU was thought to be significant enough to depict the occurrence of scintillations. The research findings would be useful to aviation industry, the marine industry, the communication service providers and other technological systems whose operations may be affected by the space weather conditions.

CHAPTER ONE

1.0 INTRODUCTION

1.1 Background Information

The Sun emits highly conducting plasma at speeds of about 500 kms^{-1} into the interplanetary space because of the supersonic expansion of the solar corona. This plasma is called the solar wind and it consists mainly of electrons and protons, with an admixture of 5% Helium ions[1]. Because of its high conductivity, the solar magnetic field is frozen in the plasma and drawn outward by the expanding solar wind. The solar wind plasma cannot easily penetrate the terrestrial magnetic field and so when the solar wind hits the Earth's magnetic field, it is slowed down and deflected around it. This is a consequence of the fact that the interplanetary magnetic field lines cannot penetrate the terrestrial field lines, i.e. the Earth is protected from the solar wind by its magnetic shield called the magnetosphere. However when the solar wind particles impinge on the terrestrial magnetic field. They get to gyrate about the field lines from North to south, back and forth and occasionally leak into the earth's lower atmosphere at the poles. This leads to an observed glow at the poles known as aurora. The leakage of these particles into the Earth's atmosphere could lead to geomagnetic storms. Geomagnetic storms could cause disruption of communication systems, cause errors in positioning as given by the Global Navigation Satellite Systems (GNSS) as well as overload of the power grid, leading to transformer shut down and power blackouts, among other effects on technological systems.

When the solar ultraviolet ray impinges on the Earth's atmosphere, it ionizes a fraction of the neutral atmosphere. At altitude of about 80km, collisions are too infrequent to result in rapid recombination and permanent ionized population called the ionosphere is formed. The ionosphere is divided into three layers D, E, F; with

each layer referring to ionization within a region as shown in Figure 1. Each region is characterized by a local maximum in the number density of ions.

The D region, the lowest ionospheric layer, extends from approximately 50 to 90km. The main sources of ionization in the D region are solar UV photons ionizing nitric oxide (NO) molecules. During solar maximum conditions, solar hard X-rays ionize air molecules (molecular nitrogen and oxygen). In addition, cosmic rays produce ionization at this altitude. Because the neutral density is relatively high in the D region, the amount of recombination is very great. Therefore, the D region is essentially only present during the day (though cosmic rays produce a residual level of ionization at night), and the level of ionization in the D region is the lowest of the different regions of the ionosphere. Solar storms can emit large amounts of X-rays that can cause rapid increases in D region ionization (sudden ionospheric disturbances (SIDs)). The D region is important with regard to high frequency (HF) radio communication because it absorbs radio waves, which causes degradation of long-distance HF communication. During SIDs and intense polar cap precipitation of solar energetic particles, D region ionization can become so intense that HF radio communication is completely blocked out[2].

The next layer moving up in altitude is the E region. It extends from 90 to 120 km and is formed by both low energy (or soft) X-rays and UV solar radiation ionization of molecular oxygen (O_2). The peak density in the E region is over a 100 times greater than the peak density in the D region because recombination is less prevalent at these high altitudes. As with the D region, the E region decays away at night, which effectively raises its height owing to high recombination rates and it decays away more quickly at low altitudes than at higher altitudes. Besides solar photons, E region ionization also occurs due to energetic particles precipitating into the atmosphere. Particle precipitation is particularly important at high latitudes. Impact of ionization causes visible light to be emitted (the aurorae). The aurorae, which appear as ovals in the high latitude northern and southern hemisphere, are some of the most beautiful natural color and light shows. Particle precipitation-induced ionization

increases the E region ionosphere substantially, particularly at night when photo production is absent. There are other, more transient sources of ionization at E region heights, including complex dynamics resulting from the effects of neutral atmosphere motion, auroral electric fields, and meteors entering the upper atmosphere that oblate (or burn up) and impact the surrounding neutral gas with enough energy to create an ionized trail. These sources produce narrow, short-lived regions of high-density ionization at E region altitudes, known collectively as Sporadic E. The mechanisms responsible for Sporadic E depend on latitude. Sporadic E can last from a few minutes to several hours. Ionization can be locally very high, and therefore, high-frequency radio waves can be reflected off these trails for long-distance communication[2].

The densest region of the ionosphere is the F region. It extends from 120 km and usually peaks at 300 km. In the region above the peak, called the topside ionosphere, the density slowly decreases and blends into the magnetospheric region called the plasmasphere. The transition between the topside ionosphere and the plasmasphere is typically at about 1000 km and is marked by the transition from oxygen as the dominant ion in the ionosphere to hydrogen as the dominant ion in the plasmasphere. The F region is formed by extreme UV solar radiation ionizing atomic oxygen. F layer ionization decreases at night, but not as much as the E and D layer ionization because at this higher altitude recombination rates are lower, and the layer consists of atomic oxygen rather than the molecular ions that dominate in the D and E regions. Atomic ions have much lower recombination rates in general than molecular ions. The F layer divides into two layers during the day because of the enhanced photoionization at high altitudes. The F2 peak is more dense than the F1 peak[2].

The ionosphere plays a very important role in satellite navigation and communications in general. However, disturbances in the ionosphere lead to distortion of trans-ionospheric signals, which has an effect of degrading the performance and reliability of communication, and navigation systems both from the

ground stations and from those mounted on space borne vehicles. Monitoring of disturbances or irregularities in the ionosphere can be accomplished using GNSS. The integrity and continuity of GNSS services are of vital importance for the modern world civilian and military applications. However, GNSS reliability can be affected because of incorrect satellite ephemerides, which induce errors in the satellite positioning from the user point of view, poor geometry of the satellite constellation and variability in the ionosphere's Total Electron Content (TEC). In particular, the errors in positioning arise from signal delays in the ionosphere caused by refraction and scattering (dispersion) of the signals. The extent of the scattering depends on the number of electrons encountered along the signal path known as the TEC. Therefore, to correct for ionospheric delays, TEC must be broadcast to single frequency users.

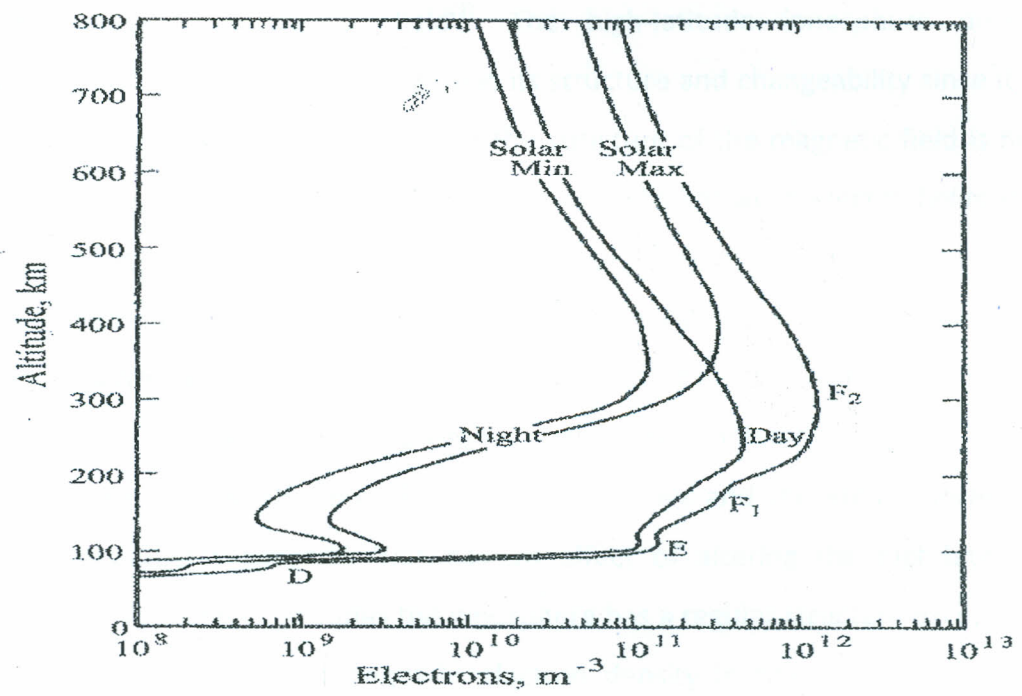

Figure 1: Electron density profile against altitude [3]

During severe geomagnetic storms, the ionosphere becomes more dynamic, turbulent, and so in addition to refraction and dispersion, a phenomenon known as scintillation can also severely affect the incoming signal. Amplitude and phase scintillation is the time variations of amplitude and phase on a signal receiver caused by the movements of irregularities and satellites[4]. While TEC in the ionosphere

affects positioning for single frequency receivers, TEC gradients and irregularities compromise integrity. Scintillations and Faraday rotation in the ionosphere can even interrupt continuity and availability of Satellite Navigation (SN) system. In Faraday rotation, a linearly polarized wave has its plane of polarization rotated as it propagates through the plasma[5]. In the existing SN systems, efforts are now being focused on putting in place a warning system for these severe space weather conditions. Scintillations are strong at high latitudes, weak at middle latitudes and intense at the equatorial region[6].

The ionosphere can be sub-divided into three major geographical regions namely: equatorial, mid-latitudes and high latitudes ionosphere. The high-latitude ionosphere is further sub-divided into the auroral and polar cap ionosphere. These classifications are based on ground observations and are mainly associated with the structure of the geomagnetic field[7]. The high-latitude ionosphere differs significantly from the mid-latitude region in its structure and changeability since it is linked with magnetospheric region where the structure of the magnetic field is not quasi-dipolar. In the high latitude region, the effects of solar wind, electric fields and particle precipitation are most strongly pronounced and, in fact, charged particles intrude into the atmosphere in the aurora oval and cusp regions [7, 8]. The particle intrusion is permanent but at low solar activity, the intensity of the invading flow is comparatively low and, most importantly, they are confined in space. With increasing solar activity, the intensity of the flow grows and the area covered by precipitating particles expands. This has an effect of altering the high-latitude ionosphere. In the middle latitudes the ionosphere has a regular structure except for periods of solar flares, the changes in electron density in this region, generally depend on short wave solar radiation and thus have a comparatively regular structure [7]. The equatorial ionosphere also has its specific features; the global scale dynamo action generated by the midday eastward polarization field at the dip equator gives rise to a downward hall current. This leads to setting in of a strong vertical polarization which opposes the downward flow of current giving rise to a very intense hall current normally termed as the equatorial electrojet (EEJ)[3, 7]. The

EEJ causes intensive upward electrodynamics plasma flow from F region heights up to 500—600 km from where the charged particles spread along field lines to both southern and northern hemisphere reaching the top height F-layer ionosphere at about 20^{o} latitude. Hence, in daytime conditions, there is minimum electron density close to the geomagnetic equator, and increased electron density on both sides of the equator[1, 7].

It is observed that instead of the electron density coming to a maximum over the equator as we might expect, there is actually a minimum over the equator and two maxima 10^{0}-20^{0} north and south of the equator[9]. This is the phenomenon called the Equatorial Ionospheric Anomaly (EIA). The equatorial anomaly is caused by worldwide solar driven winds, which result in the solar quiet current system in the E-region of the earth's atmosphere at about 100—130 km altitude. Resulting from this current is an electrostatic field directed East-West in the equatorial dayside of the ionosphere. At the magnetic dip equator where the geomagnetic field is horizontal, this electric field results in an enhanced eastward current flow within $\pm 5^{o}$ of the magnetic equator commonly known as the EEJ[9]. This phenomenon can be illustrated as shown in Figure 2.

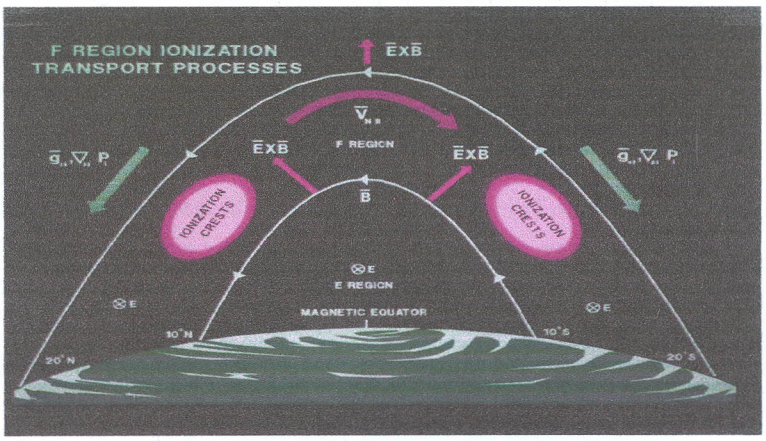

Figure 2: Equatorial Anomaly [8]

From the Figure 2, it is observed that near the magnetic equator the electric field lines of the atmospheric global current in the E-layer are pushed upwards across geomagnetic field lines to the F-layer where they produce an upwards movement of

the plasma during the day. The raised plasma then diffuses down along field lines to produce enhanced density at places on each side of the equator and decreased density at the equator itself [9]. Part of Kenya though lies within the anomaly region and experiences this phenomenon. Figure 3 shows the major geographical regions of the ionosphere and the equatorial anomaly.

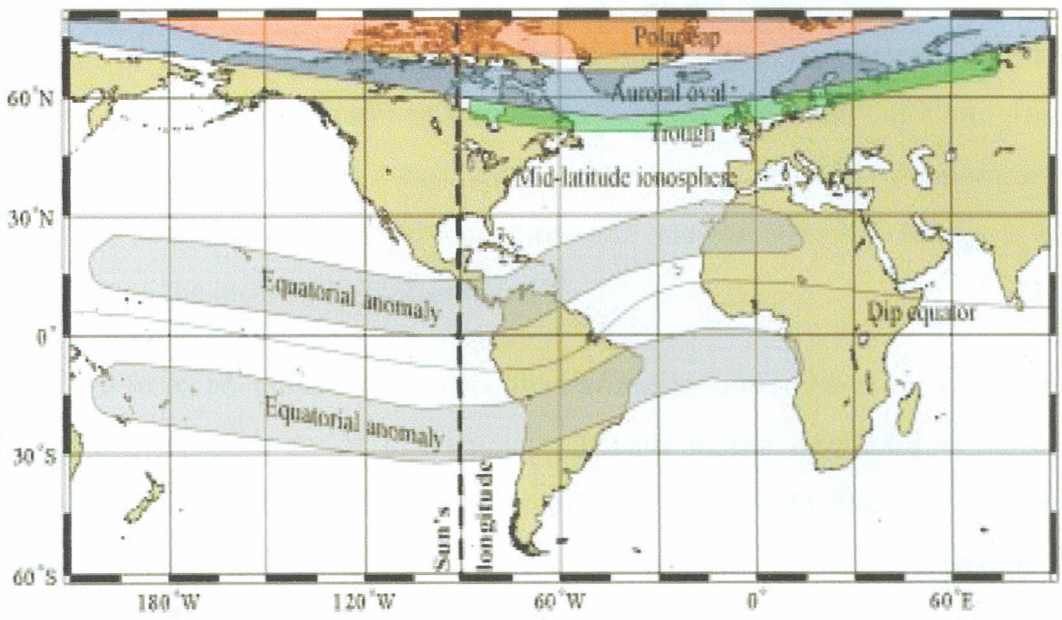

Figure 3: Geographical regions of the ionosphere showing equatorial anomaly[2]

1.2 Ionospheric measurements

To monitor the physical parameters of the ionosphere two types of general techniques exist: in—situ measurements (airglow imager and rockets) and remote sensing observation (e.g.: ionosondes, coherent/incoherent scatter radar, GNSS receivers network, magnetometers). Each of these techniques has its own advantages and disadvantages.

The in-situ measurements such as the airglow imager and rockets normally are used in measuring the intensity of the gravity waves. Zuzuki, S. et al. (2007) and Stockwell, R. G. and Lowe, R. P. (2001) used such method to identify small-scale (20–100 km) atmospheric gravity waves from OH airglow images to estimate momentum fluxes carried by the waves[10,11].

The remote sensing observation is used in study the electron density in the ionosphere. The ionosondes and coherent/incoherent scatter radar, at times called bottom sounders are best in plotting the electron density profiles. Incoherent scatter radar theory involves a ground-based technique for studying the Earth's ionosphere. A radar beam scattering off electrons in the ionospheric plasma creates an incoherent scatter return. The distribution function of the ionospheric electrons is modified by the much slower and massive positive ions — electron density fluctuations relate to ion temperature, mass distribution, and motion. The incoherent scatter signal allows measurement of electron density, ion temperature and electron temperatures, ion composition and plasma velocity. Figure 1 is obtainable using the incoherent scatter radar[12].

In its simplest form, an ionosonde consists of a transmitter and receiver with coupled tuning circuits, which is swept in frequency (usually in the frequency range of approximately 0.5–25 MHz). It can be either a pulsed or a CW-FM (chirp) system, and the transmitter and receiver can either be co-located (monostatic) or separated (bistatic). After the RF signals have been reflected by the ionosphere they are received and processed by the receiver to produce ionograms. The basic information in the received signal is the transit time for passage between ionospheric layers and the Earth, frequency, amplitude, phase, polarization, Doppler shift, and spectrum shape. From these quantities, we can obtain an ionogram, which is a plot of the virtual height of reflection versus frequency. We can also deduce the true height of ionospheric layers as a function of frequency, the line-of-sight (LOS) velocity, some communication parameters, and the vector velocity of ionospheric irregularities (with an array of several antennas)[12].

The GNSS involves the use of satellites, which transmit signals. The signals pass through the ionosphere and before being received by ground based receivers.

Usually observations from both techniques, in—situ measurements and remote sensing observation, are required to provide a comprehensive understanding of the ionosphere and its physical processes. Among the Remote sensing methods that use

radio waves the most widely applied are: bottom side soundings (from the ground), topside soundings (satellite borne), TEC measurements and incoherent scatter radar.

The TEC is obtained from data gathered by GNSS receiver stations. The data is received from several satellites. It is then archived in a format called Receiver Independent Exchange (RINEX) format. This data can be processed to obtain information about TEC in that locality.

The TEC is the number of electrons in a column of one metre—squared cross—section along a trans—ionospheric path.

$$N_T = \int_S N(S)ds \tag{1}$$

$$1TEC\ unit\ (or\ TECu) = 10^{16} electrons/m^2 \tag{2}$$

1.2.1 Ionospheric TEC measurements using the dual frequency GPS signals

The Slant Total Electron Content (STEC) is the measure of the total number of free electrons in a column of the unit cross section along the path of the electromagnetic wave between the satellite and the receiver[6]. The total number of free electrons is proportional to the ionospheric differential delay between L1 (1575.42 MHz) and L2 (1227.60 MHz) signals.

$$STEC = \int_{receiver}^{satellite} Nds \tag{3}$$

where N is the electron density; 1 TEC Unit = 10^{16} electrons/m^2.

In practice, STEC is obtained from the dual frequency code measurements, given by

$$STEC = \frac{1}{40.3} \times \left(\frac{1}{L_1^2} - \frac{1}{L_2^2}\right)^{-1} \times (P_1 - P_2) + TEC_{CAL} \tag{4}$$

Where P1 is the pseudo range at L1, P2 is the pseudo range at L2 and TEC_{CAL} is the bias error correction and is different for different satellite–receiver pairs.[6].

In their study, Bagiya et al. (2009) corrected the receiver part of the above bias by taking the value of 0.793 TECU supplied by the manufacturer by calibrating the

receiver against Wide Area augmentation system (WAAS). As they were mainly concerned with variations of TEC, the above approach was satisfactory. This procedure gave the corrected slant TEC[6].

As STEC is dependent on the ray path geometry through the ionosphere, it is desirable to calculate an equivalent vertical value of TEC which is independent of the elevation of the ray path. The Vertical Total Electron Content (VTEC) is obtained by taking the projection from the slant to vertical using the thin shell model assuming a height of 350 km, following the technique given by (Klobuchar, 1986):

$$Vertical\,TEC(VTEC) = STEC \times Cos\left[arc\,sin\left(\frac{R_e cos\theta}{R_e} + h_{max}\right)\right]$$

where R_e is the radius of the earth and is taken as 6378 km, h_{max} is the maximum height of the ionosphere expected and is taken as 350 km and θ is the elevation angle at the ground station[13].

Rama Rao et al. (2006) observed that the Ionospheric Pierce Point (IPP) altitude of 350 km is valid for the Indian region for satellite elevation angle greater than 50°. For the satellite elevation angle lower than the 50°, they further showed that the calculated VTEC is critically dependent on the IPP latitude[14].

1.3 Ionospheric variations

Two major forces cause dynamic variations of the ionosphere. They are North–South neutral winds, which are slow variations that propagate latitudinally, and East–West Electric field, which are fast variations that are simultaneous on global scale and are associated with geomagnetic disturbances.

The ionosphere displays marked variations with altitude, latitude, longitude, universal time, season, solar cycle, and magnetic activity. The variations are shown in all ionospheric properties: electron density, ion and electron temperatures and ionospheric composition and dynamics. This is primarily a result of the ionosphere's coupling to the other regions in the solar-terrestrial system: the sun, the

interplanetary medium, the magnetosphere, the thermosphere and the mesosphere and (to a certain extent) the stratosphere and troposphere.

These variations are of two general types, regular and irregular. Regular variations, occur in cycles and can be predicted in advance with reasonable accuracy (quiet ionosphere) while irregular variations are mostly related to the irregular behavior of the sun and so cannot be easily predicted in advance.

Regular time variations that affect electron density in the ionosphere can be divided into these main classes: diurnal, day-to-day, seasonal solar activity.

1.3.1 Diurnal Variation

Electron density in the D region disappears at night. Electron density in the E and F1 regions depends on the angle of the sun (Chapman layers) and is greatly reduced at night. The electron density in the F2 region is highly variable and its diurnal variation depends on season, solar activity and geographical position.

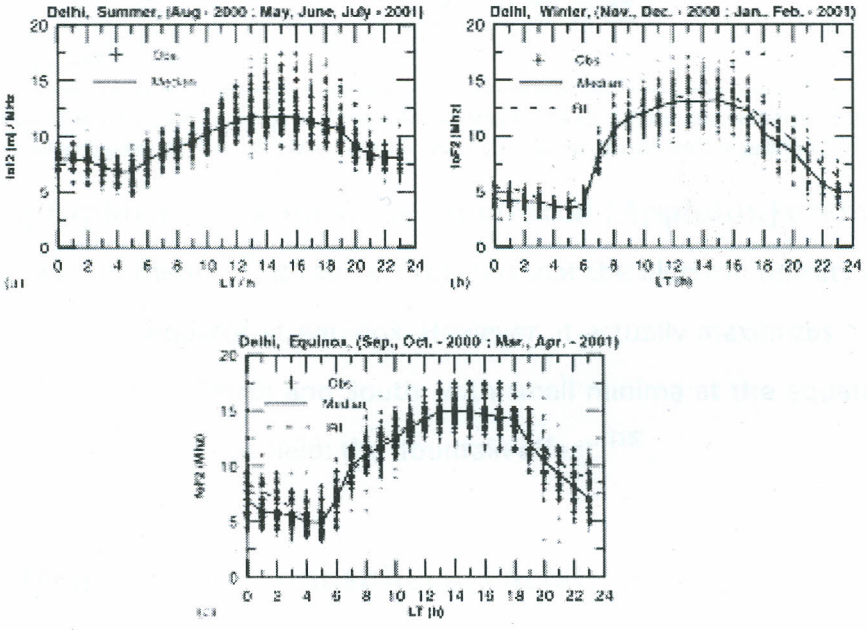

Figure 4: Scatter plot showing diurnal variation of foF2 derived from the digital ionosonde at Delhi for (a) summer, (b) winter and (c) equinox. The median values are shown as solid line. The IRI model values are shown as dash lines [15]

Figure 3 shows a scatter plot showing diurnal variation of the peak plasma frequency of the F2 region (foF2) derived from the digital Ionosonde at Delhi for, summer,

winter and equinox. The median values are shown as solid lines. The International Reference Ionosphere (IRI) model values are shown as dash lines.

1.3.2 Solar activity variations

Sun spot numbers determine the extent of solar activity during a given period of the year or during a given year. Figure 5 shows a typical electron density profiles at three solar activity levels for winter and summer noon conditions at Washington DC (Belvoir).

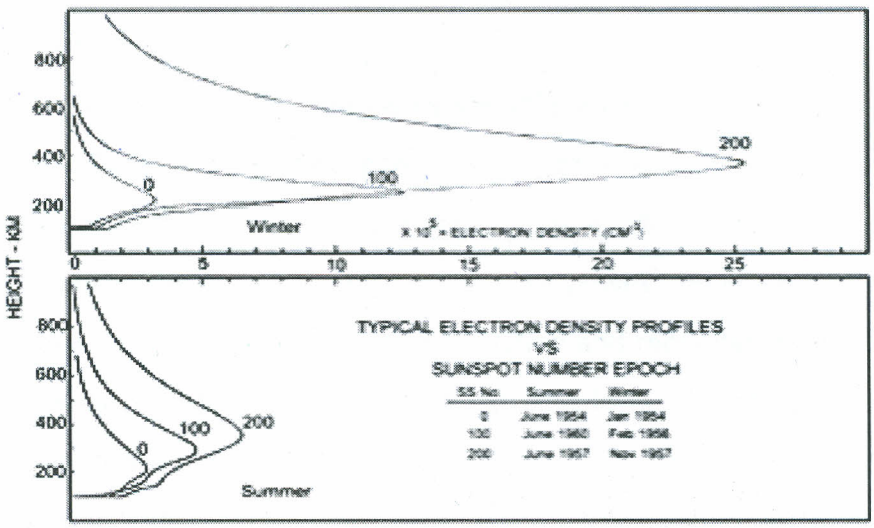

Figure 5: Typical electron density profiles at three solar activity levels for winter and summer noon conditions at Washington DC (Belvoir). Magnetically quiet days were chosen for the profiles [16]

1.3.3. Geographical variations: the equatorial (Appleton) anomaly

From the Chapman theory[17], it can be expected that the electron density maximize over the geographic equator at equinox. However, it actually maximizes ~ 10°—20° of geomagnetic latitude North and South, with small minima at the equator due to the effect of the geomagnetic field: the 'fountain effect' [18].

1.4 Consequences of Ionospheric Variations

1.4.1. Scintillations

A radio wave crossing the upper and lower atmosphere of the Earth's atmosphere suffers a distortion of phase and amplitude. When it traverses drifting ionospheric irregularities, the radio wave experiences amplitude and phase fluctuations, which

not only vary widely with its frequency, but also with magnetic and solar activity, time of day, season and location. These effects are called amplitude and phase ionospheric scintillations. Scintillations are caused by scattering of radio wave by free electrons in the ionosphere and may be weak or strong. The strongest scattering is observed in the equatorial and auroral regions, and the severity of scintillations is experienced much more at night than at any other time. This may lead to disruption of communication systems and compromise the integrity of GNSS Systems, which is very crucial for military surveillance and safety in the aviation industry[19].

1.4.2 Ionospheric Storms

Ionospheric storms are driven by highly variable solar and magnetospheric energy inputs to the Earth's upper atmosphere. During geomagnetic storms, the disturbed solar wind compresses the Earth's magnetosphere. The disturbed thermospheric circulation alters the neutral composition, and moves the plasma up and down magnetic field lines, changing rates of production and recombination of the ionized species. Ionospheric storms represent an extreme form of "space weather", which can have significant, adverse effects on telecommunication and navigation systems. These effects include errors in GNSS systems positioning application and in Very Low Frequency (VLF) navigation systems, loss of lock in HF communications, and disruption of Ultra High Frequency (UHF) satellite links[20].

The ionospheric variations lead to variability of the TEC, which makes it hard to predict the space weather condition. The variability of the TEC makes it difficult to use models like the IRI 2007 to predict the ionospheric conditions at any given time. This is particularly true with the ionospheric storms, which therefore poses uttermost challenge to communications systems and other systems, which are affected by space weather.

1.5 Statement of Problem

It is clear from the foregoing discussion that the variability of the TEC is a concern which needs to be addressed. It is rightly observed that the day-to-day variability of

the TEC remains unresolved even after several decades of research [21]. The highest value of TEC in the world are found in the equatorial region; but comparatively, little corresponding research has been done on the low latitude (equatorial) ionosphere [19], and especially in Africa where ground based equipments have been lacking for quite a long time and the few which have been there have not been in consistent operation. Some of the major reasons for the sorry state of the few equipments that have been available include technical challenges as well as frequent power failure. Figure 85 in Appendix V shows the distribution of the IGS stations in the world as at February 2013. The equipment density in the East African sector is lower compared to South African, American, Asian and European sectors and this necessitates concerted efforts to deploy more observing facilities in this region in order to better understand the dynamics of the ionosphere in this region.

The effects of the ionospheric variability, which cause significant effects on satellite signals for communication and navigation, are much more severe in the equatorial region even for magnetically quiet days [16]. This research was conducted to study and monitor activity on TEC and TEC variability, which may cause ionospheric scintillation over Malindi using Global Positioning System (GPS) measurements obtained from Malindi (3°12'57.93" S, 40°06'34.99" S) and then characterize the day-to-day variability seasonal variability and solar maximum type variability. The study was focused to capture the peak of the 23rd solar cycle, that is 1999, 2000, 2001 and 2002.

1.6 Justification of Study

The ionosphere plays an important role in satellite radio communication and navigation and its density determines the lifetime of Low-Earth Orbiting (LEO) satellites. An understanding of the ionospheric TEC variability will improve our understanding of the space environment (space weather) around the equatorial region and more so in Kenya.

Space weather has broad impacts on humans and technological systems. Such include intense radiation exposure to astronauts and airline crew on polar routes which result in death, damage to satellite hardware leading to huge economic losses and degradation of biological systems navigation abilities e.g. the degradation of homing pigeons' navigational abilities during geomagnetic storms. Pigeons and other migratory animals, such as dolphins and whales, have internal biological compasses composed of the mineral magnetite wrapped in bundles of nerve cells.

Many communication systems use the ionosphere to reflect radio signals over long distances. Ionospheric storms affect radio communication at all latitudes. Some radio frequencies are absorbed and others are reflected, leading to rapidly fluctuating signals and unexpected propagation paths e.g. ground-to-air, ship-to-shore, shortwave broadcast, and amateur radio (mostly the bands below 30 MHz) are frequently disrupted. Radio operators using HF bands rely upon solar and geomagnetic alerts to keep their communication circuits up and running. In addition, some military detection or early warning systems are also affected by solar activity. The *over-the-horizon radar* bounces signals off the ionosphere to monitor the launch of aircraft and missiles from long distances. During geomagnetic storms, this system can be severely hampered by radio clutter. Some submarine detection systems use the magnetic signatures of submarines as one input to their positioning schemes. Geomagnetic storms can mask and distort these signals. Damage to communication satellites can disrupt non-terrestrial telephone, television, radio, and Internet links.

GNSS are adversely affected when solar activity disrupts their signal propagation. Airplanes and ships use the very low frequency signals from these transmitters to determine their positions. During solar events and geomagnetic storms, the system gives navigators information that is inaccurate by as much as several miles. If navigators had been alerted that a proton event or geomagnetic storm was in progress, they could have switched to a backup system. GPS signals are affected when solar activity causes sudden variations in the density of the ionosphere, causing the GPS signals to scintillate (like a twinkling star). The scintillation of

satellite signals during ionospheric disturbances can lead to large errors in positioning applications e.g. surveying, car tracking etc. Geomagnetic storms can affect power grid. The currents induced in these lines from geomagnetic storms are harmful to electrical transmission equipment, especially generators and transformers — induces core saturation, constraining their performance (as well as tripping various safety devices) and causes coils and cores to heat up. This heat can disable or destroy them, even inducing a chain reaction that can overload and blow transformers throughout a system. Rapidly fluctuating geomagnetic fields can also produce geomagnetically induced currents in pipelines. This can cause multiple problems for pipeline engineers. Flow meters in the pipeline can transmit erroneous flow information, and the corrosion rate of the pipeline is dramatically increased. Accordingly, such harmful effects have been usually observed only at high geomagnetic latitudes (such as in Canada or Scandinavia), because it is at the regions dominated by the auroral ionospheric currents where the ground magnetic field variation signatures reach the highest amplitudes. Nevertheless, large GICs have been measured at any latitude, even at equatorial locations [23]. If engineers incorrectly attempt to balance the current during a geomagnetic storm, corrosion rates may increase even more. Thus, pipeline managers need to receive space weather alerts and warnings to allow them to implement defensive measures.

1.7 Justification of the Study Site

There are two IGS stations in Kenya, Malindi (code name, mal2) and Nairobi's Regional Centre for Mapping and Navigation (code name rcmn). There are three SCINDA TEC receiver stations in Kenya. These include the Nairobi University TEC receiver station, Jomo Kenyatta University TEC receiver and Maseno University receiver station.

Malindi IGS was considered as the source of data because of three major reasons. First, the data gathered from it was freely available to any interested researcher. Secondly, it had long history of existence, having been operational for the past two decades. Some information from the internet indicate that Malindi IGS was

established by the German Government in the year 1995 under the four letter code name *"mali"*. The receiver type was ROGUE SNR-8C Serial Number 303 and Firmware Version MEENIX 7.8 / RUSE 4.2. It has since then been updated, and in 2001, a newer version of receiver type ASHTECH Z-XII3, Serial Number, LP020005006, Firmware Version, NAV CD00,CHN 1D02*21, was installed[24].

The Nairobi's 'rcmn' was established in 1996. However the data for the years we wanted to study could not be obtained from the internet for reasons whichwewas not able to establish. Finally, Malindi had history of high percentage of data availability (80%) as compared to Nairobi 'rcmn', located at Kasarani, just at the outskirts of Nairobi, whose data availability was averagely 60%. The SCINDA receiver stations were private and therefore the data usage was highly restricted.

It is not clear when Addis Ababa IGS station, code name 'adis', started operating. From the web it is observed that in a joint effort of Geophysical Observatory of Addis Ababa University (GOAAU), Federal Agency for Cartography and Geodesy, Frankfurt am Main (BKG), and Institute of Physical Geodesy, Technische Universität Darmstadt (IPGD) a continuously operating GNSS reference station was been established at the Addis Ababa University in Ethiopia. It was been accepted by the IGS in July 2007[25]. This means that during the period covered by this work, it was not possible to compare the results with the findings from Addis Ababa. Mbarara IGS station, code name 'mbar', similarly was not having archived data available for the public.

1.8 Significance of the Study

This study would be particularly helpful in developing a morphological description of TEC that would be useful in the understanding of the space weather conditions over Kenya. The information would be made available to the aviation industry, the marine industry, the communication service providers and many other establishments whose operations could be affected by the space weather conditions. In the aviation and marine industries, predicting the TEC variability is vital for safety given that ionosphere aided communication rely on it.

1.9 Objectives of the Study

The objectives of the study were to:

(i) Obtain plots of TEC against time of the day and TEC against day of the year, from which we study day-to-day variability and seasonal variability respectively during the solar maximum of the 23rd solar cycle, i.e. 1999, 2000, 2001 and 2002.

(ii) Characterize the various types of TEC variability to come up with a morphological description of TEC that may be useful in the understanding of the space weather conditions over Kenya during the solar maxima.

1.10 Scope of the Study

This study samples four months for years 1999, 2000, 2001 and 2002. These are, January, April, July and October. The months represent four seasons, March equinox season (March, **April**, May), June solstice season (June, **July**, August), September solstice season (September, **October**, November) and December Solstice season (December, **January**, February). It is of interest to know particularly what happens during the equinoxes and the solstices. The equinoxes when the sun crosses exactly over the equators, are on the 21st March and 23rd September. The months of April and October are the best choices to study the variability of the ionosphere. The December solstice happens on the 22nd December. This makes January to be the most suitable month for studying the impact of the solar wind on the ionosphere during that period. We have the June solstice taking place 21st June. Similarly, the impact of the sun on the ionosphere during that period could as well be studied in the month of July.

Ordinarily, studying all the 48 months in the four years, i.e. 1999—2002 would give a more elaborate and detailed picture of variability. However, given that the study was to be exhausted only within a limited period, the sampling was done.

1.11 Limitations of the study

This kind of study would be best done if we could compare both Ionosonde TEC plots with those of GPS but we do not yet have enough Ionosonde TEC data available in Kenya. The only Ionosonde TEC receiver in the country was installed towards the end of 2012 in Maseno University, but is yet to start full operation given that the installation was not complete. The ionosonde is a device, which is generally used to profile the ionosphere. It is a vertical sounder of the ionosphere, which sweeps over a frequency range of 1-20 MHz and works on the principle of reflection[26]. Given the dispersive nature of the ionosphere, the height we obtain is called the virtual height. To obtain the real height from this virtual height, one has to use numerical methods and the commonly used method is the Polynomial Analysis (POLAN)[27]. From ionosonde profiles, we also obtain the peak frequency and peak heights which correspond to the plasma frequency and height of the maximum electron density at that epoch respectively. This peak height is observed to be not constant in time and these peak heights obtained from the ionosonde were used as shell heights in our analysis of the GPS data.

The second limitation was occasional lack of data; for example, April 2001 lacked data.

CHAPTER TWO

2.0 LITERATURE REVIEW

By the year 1920, ionospheric physics was already an area of interest for study. It is worth noting that in the years following the founding of the Observatori de l'Ebre (or in Spanish, Observatorio del Ebro)—1904, situated in Spain, the quick evolution of the knowledge on the influence the Sun's activity has on terrestrial physics led the Observatory to concentrate on some particular problems [28]. In 1920, the director of the center, the Jesuit Lluís Rodés (1881–1939) introduced, among other topics, the study of magnetic storms and rapid variations of the magnetic field [29].

Rodés was aware of the contemporary knowledge of the ionosphere. In his analysis about the simultaneity of magnetic storms [29] he already points to the necessity of taking into account the contributions of the ionized atmosphere. He published two different editions of a popular science book titled "El Firmamento" [28]. In the first edition is a description of the structure of Earth's atmosphere without any mention of an upper ionized layer. In contrast, the second edition explains this upper ionized layer, and even gives the principles of the vertical ionospheric sounder [28].

Another related topic that was studied during those years was the periodicity of the variations of the atmospheric electric potential field. Daily variations and other short period regular variations carefully studied at the Observatory were directly connected with ionosphere dynamics [28].

In the equatorial region during the daytime, dynamo electric fields in the off equatorial E-region locations move along the magnetic field to F-region heights at the magnetic equator and the resulting **E×B** force lifts the F-region plasma to higher altitudes. Then by action of forces parallel to **B** due to gravity and plasma pressure gradients, the uplifted plasma diffuses along the magnetic equator leaving a trough in the ionization density at the magnetic equator. Two belts of high ionization density are formed nominally around magnetic dip latitude of 15°N and 15°S. These are the crests of the equatorial ionization anomaly (EIA) [30]. At the time of sunset,

the F-region zonal neutral wind and conductivity gradient causes, the sunset terminator (a line between the day and night) to develop an enhanced eastward electric field called the pre-reversal enhancement (PRE). This causes the F region to move upward. As a result, plasma bubbles are generated [31], and irregularities ranging from hundreds of kilometers to tens of centimeters are formed. Thus, the pre-reversal eastward electric field is of crucial importance for the destabilization of the ionosphere, which in turn creates the kilometer-scale irregularities giving rise to scintillation of satellite signals [31]. This electric field also leads to a resurgence of the EIA in the post-sunset period. The result is that scintillation at frequency as high as 4 GHz can be encountered near the EIA crests during ~~a~~ solar maximum [32].

Studies have shown that scintillations at low latitudes are a serious problem for communication and GPS-based navigation because very large adverse effects are seen on these systems even for magnetically quiet days [33]. As quiet days are far more prevalent than disturbed days, it is quite possible to have scintillations at VHF on a large fraction of the days during the "scintillation season" at a given site, except for unpredictable variability [32, 34].

In their study of diurnal and seasonal variation of GPS-TEC during a low solar activity period as observed at a low latitude station, Agra, Chauhan et al., discovered that the mean TEC varies from a pre-dawn minimum to an afternoon maximum and then decreases. The low values of TEC are observed in winter whereas high values are observed in equinox and summer [35]. They observed a large variability imposed on the low latitude ionosphere during sunrise and sunset transition period. As the total magnetic field, tube is very small at equatorial and low latitudes, the electron contents in the field tubes collapse rapidly after sunset in response to low temperature in the thermosphere in the nighttime. Following the sunrise, the magnetic field tubes again get filled up rapidly because of their low volume resulting in steep increase in ionization.

Olwendo et al. in their paper presents the first results of TEC depletions and enhancement associated with ionospheric irregularities in the low latitude region

over Kenya. They detected the TEC depletions from satellite passes along the line of sight of the signal and the detected depletions had good correspondence with the occurrence of scintillation patches. TEC enhancement had been observed and is not correlated with increases in S4 index and consecutive enhancements and depletions in TEC had been observed which results into scintillation patches related to TEC depletions. The TEC depletions had been interpreted as plasma irregularities and inhomogeneities in the F region caused by plasma instabilities, while TEC enhancement had been interpreted as the manifestation of plasma density enhancements mainly associated with the equatorial ionization anomaly crest over this region[36]. The S4 index is a metric for indicating the amount of variation in the amplitude of a signal. It can be an indicator of the standard deviation of the GPS satellites received signal power as seen on the ground[36].

In their study, Bagiya et al. describe the diurnal and seasonal variations of TEC, solar activity dependence of TEC and effects of a space weather related event, a geomagnetic storm on TEC. They observed that the diurnal variation of TEC showed pre-dawn minimum for a short period of time, followed by a steep early morning increase and then reaches maximum value between 14:00 LT and 16:00 LT. The mean diurnal variations during different seasons were brought out. It was found that TEC at Rajkot, which was used for the study was at its maximum during Equinoctial months (March, April, September, October), and minimum during the Winter months (November, December, January, February), with intermediate values during Summer months (May, June, July, August), showing a semiannual variation. TEC values had been decreasing since 2005, onwards showing positive correlation with solar activity[37].

Rama Rao et al. in their paper present the temporal and spatial variations in TEC. This was derived from the simultaneous and continuous measurements made using the Indian GPS network of 18 receivers located from the equator to the northern crest of the EIA region and beyond, covering a geomagnetic latitude range of 1° S to 24° N, using a 16-month period of data for the low sunspot activity (LSSA) years of

March 2004 to June 2005. They observed that the diurnal variation in TEC at the EIA region showed its steep increase and reached its maximum value between 13:00 and 16:00 LT, while at the equator the peak was broad and occurred around 16:00 LT. A short-lived day minimum occurred between 05:00 to 06:00 LT at all the stations from the equator to the EIA crest region. Beyond the crest region the day maximum values decreased with the increase in latitude, while the day minimum in TEC was flat during most of the nighttime hours, i.e. from 22:00 to 06:00 LT, a feature similar to that observed in the mid-latitudes[38].

The causes of the TEC variability have been explored by various researches. Among the causes are the storm-generated disturbances in electric field, neutral wind, and neutral composition. The low-latitude ionosphere is characterized by the equatorial ionization anomaly (EIA) produced by the equatorial plasma fountain. These observations were made by Namba and Maeda (1939), Appleton (1946) and Duncan, (1960)[39, 40]. In addition to the electric field effects, it has also been observed that the storm-generated equatorward neutral wind also affects the low-latitude ionosphere by changing the field-aligned plasma transport or transporting the plasma from one hemisphere to the other[41].

The findings of the previous researches have shown the existence of diurnal variations, seasonal variations and solar cycle related variations. Not much research work has been done to show the variability. In this work, variability as opposed to variations has been explored.

In their paper, Bolaji et al. investigated the variability of GPS TEC at Ilorin, Nigeria, an equatorial zone, during the period of low solar activity and compared the results with previous studies. They observed that the diurnal variability of VTEC (DTEC), standard deviation (SD), and monthly median total electron content (MTEC) were characterized by minimum presunrise magnitudes, maximum daytime magnitudes, daytime depression, and postsunset depletion and enhancement. They also discovered that DTEC exhibited consistent minimum diurnal variation during presunrise hours between 05:00 and 06:00 LT, rose steeply during the sunrise period

(07:00–09:00 LT), and subsequently rose very slowly from 10:00 LT to the peak during the daytime, mostly around 12:00–16:00 LT. The MTEC minimum value is in the range of ~4–5 TECU between presunrise times of 05:00 and 06:00 LT. Maximum value of MTEC variation during the presunrise hour of 05:00 LT was observed in the month of May and has ~5 TECU, while the minimum values of MTEC at the same presunrise hour were seen in February with ~4 TECU[38].

Bolaji et al. noticed that the hour at which DTEC reached the diurnal peak varied from day to day, and its daytime magnitude was greater than its postsunset and presunrise magnitudes. From all the months, the maximum DTEC daytime magnitude range was between ~24 and ~34 TECU, while the postsunset to presunrise magnitude range was between ~1 and ~7 TECU[38] according to their scale range.

CHAPTER THREE

3.0 METHODOLOGY

3.1 Data Used in the Study

The TEC measurements were obtained from the Malindi IGS station (03.03°S, 40.13°E) in Kenya. This was done by downloading the archived data from the said station from the site, ftp://cddis.gsfc.nasa.gov/pub/gps/data/daily/. Several types of files are obtainable from the site. However, for the purpose of this study, only the Independent Exchange files (RINEX) files and the navigation files were downloaded from Malindi station, code name, *mali*.

When the files were downloaded, they were in compressed form to enhance the storage of huge amount of data. They could not however be used in the compressed form. Both the navigation and RINEX files were therefore decompressed using freely downloaded unzip software[45]. (The decompressed files occupy more space than the compressed ones.) The decompressed RINEX files were *hatanaka* decompressed using computer software. The *hatanaka*-compressed American Standard Code for Information Interchange (ASCII) format version of a RINEX OBS file is frequently used in conjunction with the UNIX compress, zip, gzip or other generalized compression utilities to create a very small file for Internet transfer[42].

The two sets of decompressed files were then processed further using computer software to obtain the data files which were then ready for making plots. The files had the columns of time and vertical TEC (vTEC), taken at a sampling rate of 10 minutes (which is equivalent to 600s). The sets of data described were obtained for January, April, July and October of the years 1999, 2000, 2001 and 2002.

The Matlab script for processing the data was written in such a way that it would automatically delete the negative TEC values given that the TEC can never be negative. The TEC values going beyond 100 TECU was also observed to be unusually even during stormy days. The script was therefore designed to exclude such

erroneous data. Appendix IV is a script which was meant to work out the variability plots. Lines 51 to 81 excludes erroneous data, i.e. negative data and ones with values going beyond 100 TECU, from being processed.

The processed sets of data were plotted to obtain plots of the daily variation of TEC for Malindi Kenya for the months of January, April, July and October of the years 1999, 2000, 2001 and 2002 in the form shown in the Appendix IV figures 70 to 84 respectively.

The same sets of data were plotted to obtain the Mass Plots of the Diurnal Variation of TEC for Malindi Kenya for the months of January, April, July and October of the years 1999, 2000, 2001 and 2002 in the form shown in figures 6 to 21 respectively. Mass plots in this case are superimposed diurnal variation curves plotted on the same pair of axes for a specified period, in this case one month.

3.2 Evaluation of Variability

The inter hour TEC variability was worked out by using the interquartile range of the data taken after every two hours. Interquartile range is the difference between the upper quartile and the lower quartile.

$$Interquartile\ range = (upper\ Quartile - Lower\ Quartile) \qquad (4)$$

The lower quartile is the median of the *lower* half of the data sorted in ascending order while the upper quartile is the median of the upper half of the data sorted in ascending order. The median divides a set of data sorted in ascending order into two equal parts while the upper quartile is the median of the second half of the data. Median divides a set of data into two equal parts [43]. Finding the interquartile range of a set of data taken after every two hours would give twelve plotting points for every 24 hours. The plotting points would be at the centre of the two-hour interval along the horizontal axes of the graphs. Only months with 15 days of data were considered for the analysis. The variability index in this case was therefore taken to be the interquartile range. The obtained interquartile ranges were plotted against days of the year in groups of five days of the selected months as shown in figures 37

to 50. In many plots, the choice of vertical scale left a large portion of the graph page unused. This was necessary to give uniform scale for TEC characteristics of all the months under study. The uniform scale makes comparison of the variability during different period possible.

We also used boxplot to study the variability. Boxplot is a tool in the Matlab, which captures the median, the lower quartile, the upper quartile, the lowest data value and the highest data value, at every single plot. Boxplot(X) produces a box plot of the data in X. On each box, the central mark is the median, the edges of the box are the 25th and 75th percentiles, the whiskers extend to the most extreme data points not considered outliers, and outliers are plotted individually. 25^{th} and 75^{th} percentiles are the lower and the upper quartiles respectively. The boxplots obtained from the data at a sampling rate of 10 minutes are indicated in figures 22 to 35.

The variability was also confirmed using the median of the TEC of the selected months taken after every two hours. This equally gave twelve points for every 24 hours. The plots were then used for analyzing the TEC variability.

The value of TEC between 0 and 20 TECU signified quiet period. This could mean that the communication involving the ionosphere could go on without interruption. TEC between 20 TECU and 40 TECU signified weak scintillation while any value above 40 TECU signified strong scintillation, which could significantly affect communication.

CHAPTER FOUR

4.0 RESULTS AND DISCUSSION

4.1 Graphical Representation of Data

The sets of raw data were plotted in monthly plots as shown in the Appendix IV, Figures 70 to 85. This was one format in which the raw data were presented to show the data availability during the period considered for research. Each pair of axes were set to take care of the 30 or 31 days of each month's data. In many plots, gaps where there. The gaps in the plots represented the days when no data was available. An example was in Appendix IV, Figure 71, which represented January 2000. In that month, data was only available for ten days. The remaining twenty-one days had no data, which translated to 32% data availability. The data gaps could be because of many factors, among them, electric power outage and equipments failure.

The maximum TEC values recorded during the period considered in the research was 120 TECU and that was in the year 2001. In October 2001, day 289, the TEC was 120 TECU. Generally, the values of TEC in April and October of the four years were higher than the other two months, January and July. This means that the TEC variations during the equinoxes were higher than the variations during the solstices. This follows from the fact that during the equinoxes the ionization rate is higher than during the solstices owing to the fact that the sun is directly above the equator. The year 2001 experienced the highest TEC variation due to its placement in the 11 years solar cycle. Figures 65 to 67 in Appendix I and II, showing sunspot index graphics indicating 11-year cycles, allude to the fact that the year 2001 was the year of solar maximum.

The same sets of data were shown as mass plots of the diurnal variation of TEC for Malindi Kenya from the year 1999 to 2002. Just like in the previous sets of plots, the scale was selected in such a manner that all were identical to enhance comparison. Each dotted line having a unique colour represents a whole day's data, bringing a total of thirty or thirty-one curves for days with 100% data availability, depending on

the number of days of the month. The superimposed plots of diurnal variation normalized to the vertical direction, were grouped in monthly intervals to cover the months under survey. The curve density was therefore proportional to the percentage monthly data availability. In cases where the curves where few e.g. in figure 12, representing January 2000, the data availability percentage was also low and when the line were dense like in figure 6, representing January 1999, the data availability percentage was high.

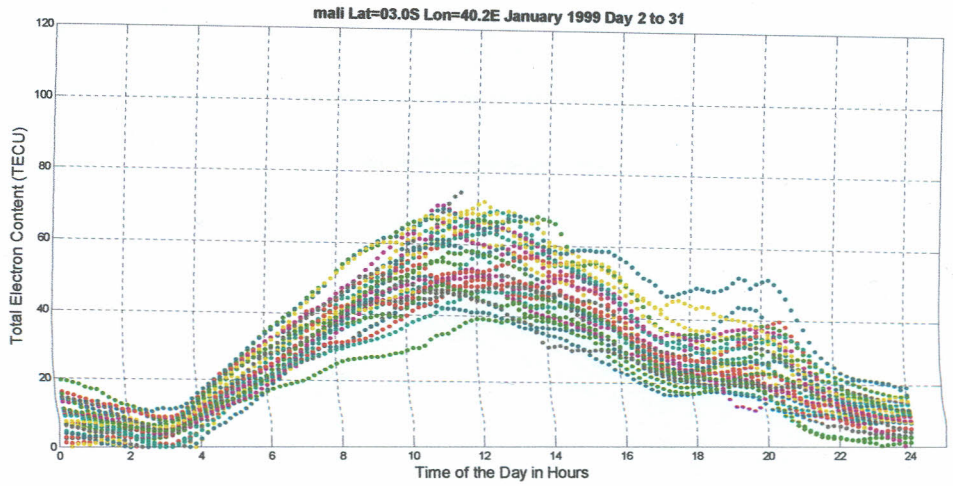

Figure 6: Monthly mass plots of the diurnal variation of TEC for Malindi Kenya for January 1999

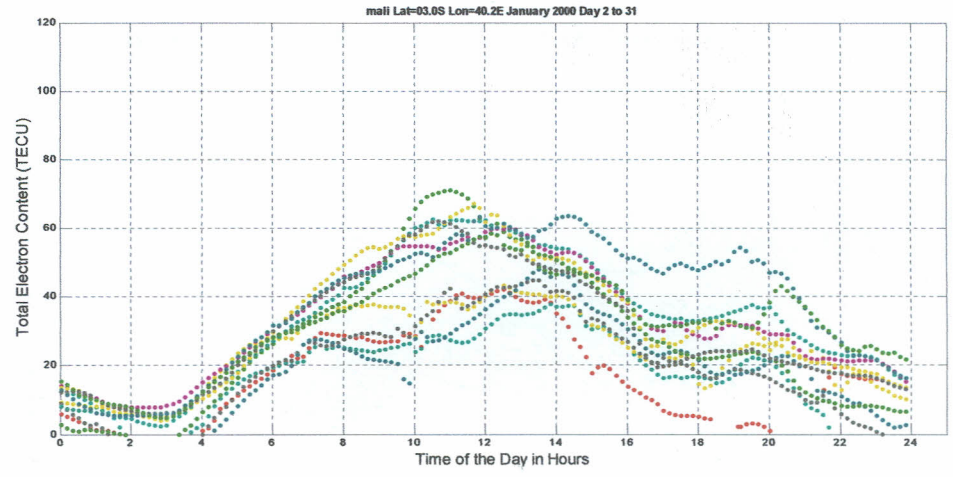

Figure 7: Monthly mass plots of the diurnal variation of TEC for Malindi Kenya for January 2000

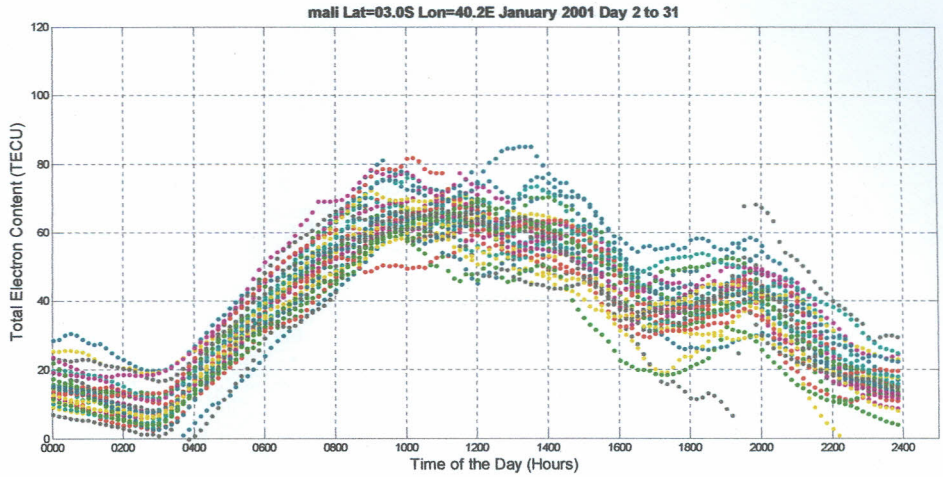

Figure 8: Monthly mass plots of the diurnal variation of TEC for Malindi Kenya for January 2001

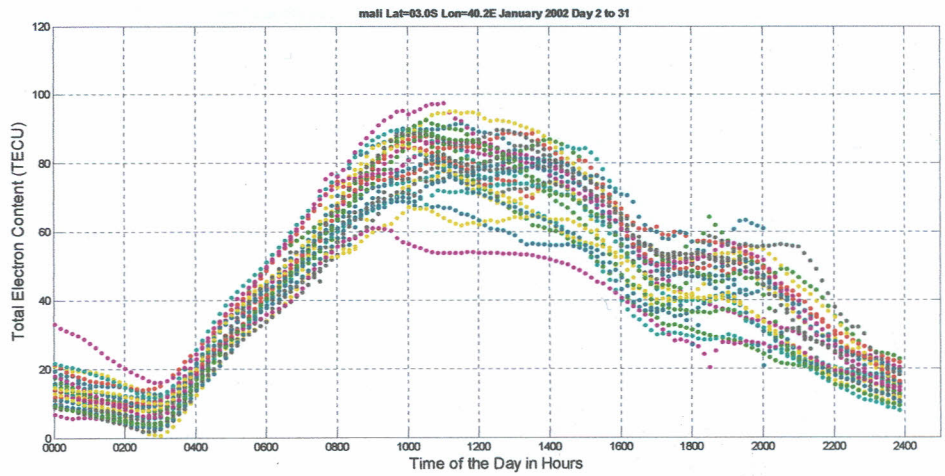

Figure 9: Monthly mass plots of the diurnal variation of TEC for Malindi Kenya for January 2002

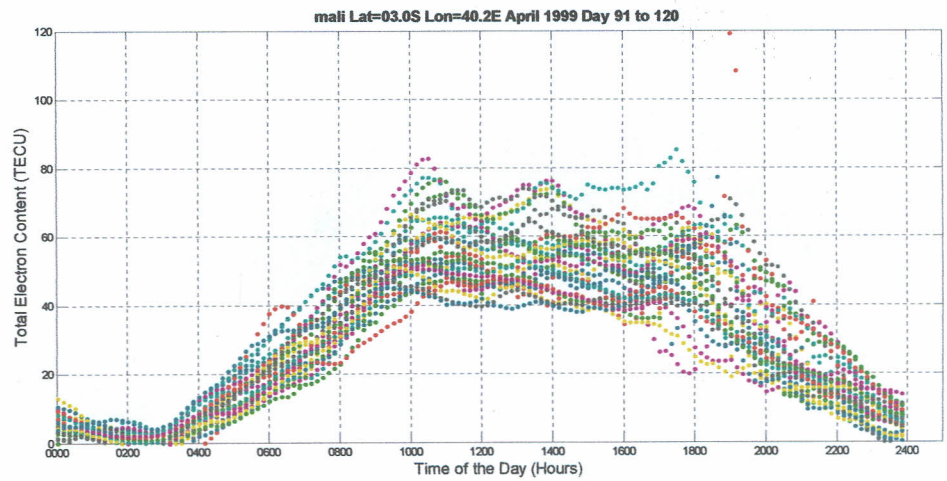

Figure 10: Monthly mass plots of the diurnal variation of TEC for Malindi Kenya for April 1999

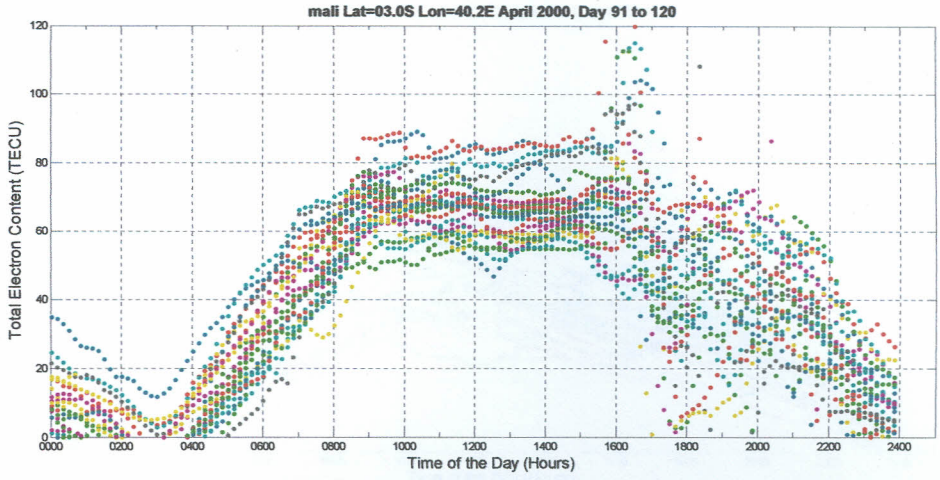

Figure 11: Monthly mass plots of the diurnal variation of TEC for Malindi Kenya for April 2000

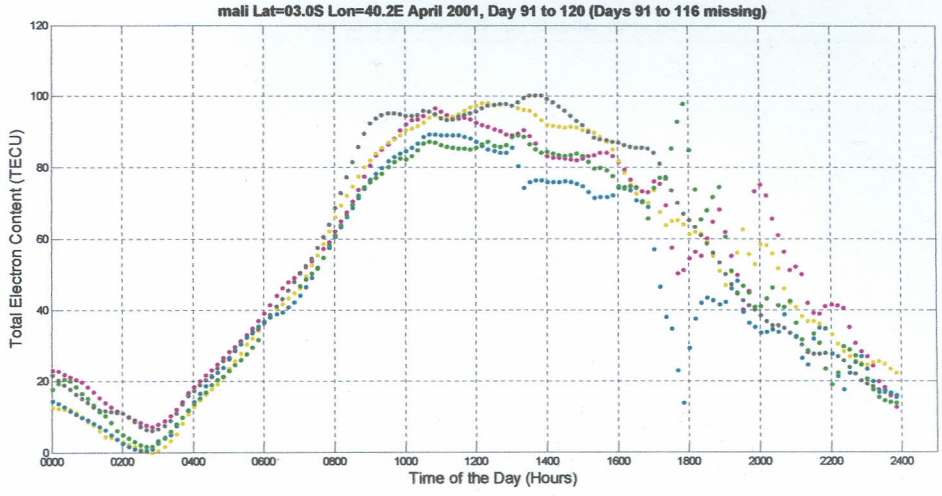

Figure 12: Monthly mass plots of the diurnal variation of TEC for Malindi Kenya for April 2001

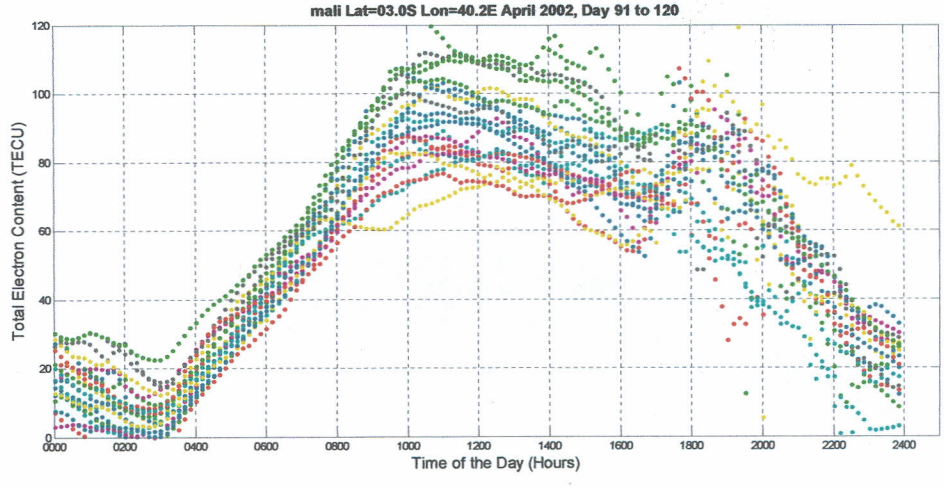

Figure 13: Monthly mass plots of the diurnal variation of TEC for Malindi Kenya for April 2002

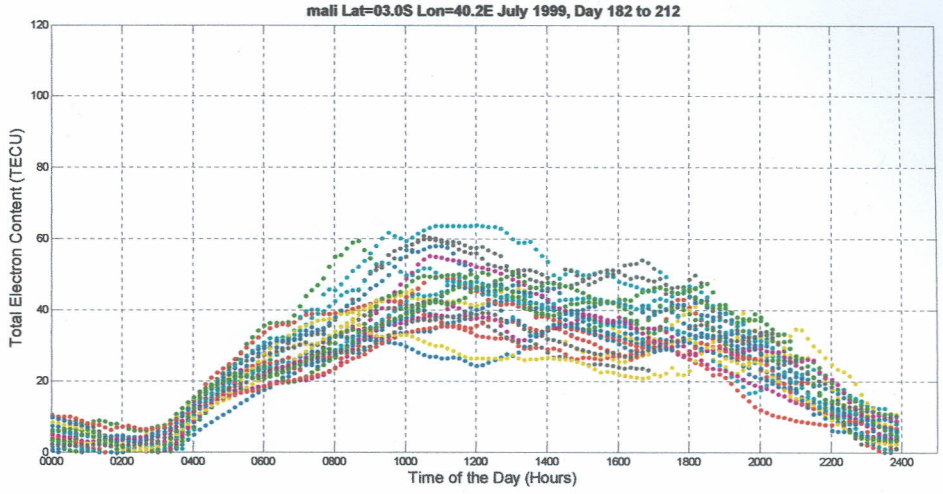

Figure 14: Monthly mass plots of the diurnal variation of TEC for Malindi Kenya for July 1999

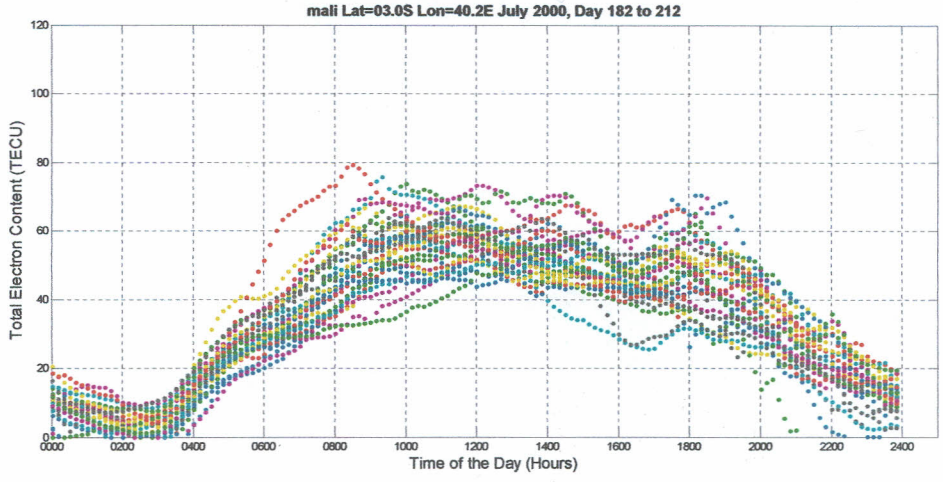

Figure 15: Monthly mass plots of the diurnal variation of TEC for Malindi Kenya for July 2000

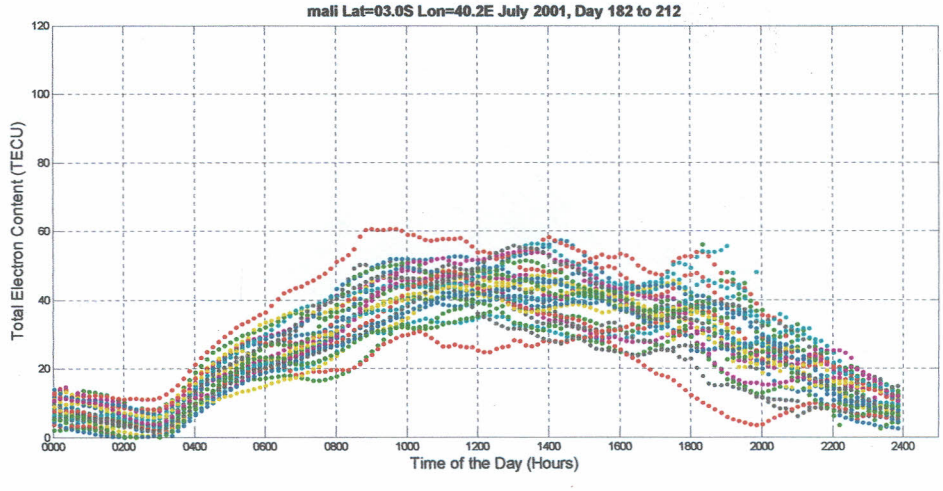

Figure 16: Monthly mass plots of the diurnal variation of TEC for Malindi Kenya for July 2001

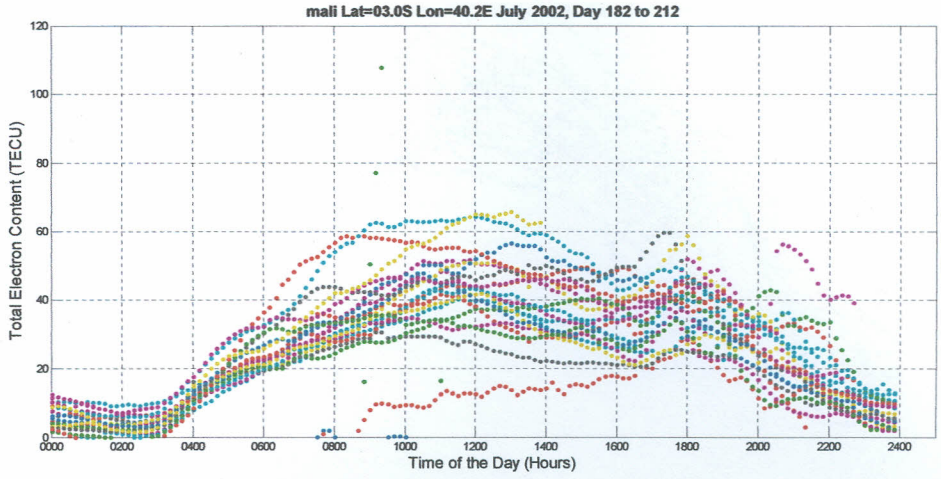

Figure 17: Monthly mass plots of the diurnal variation of TEC for Malindi Kenya for July 2002

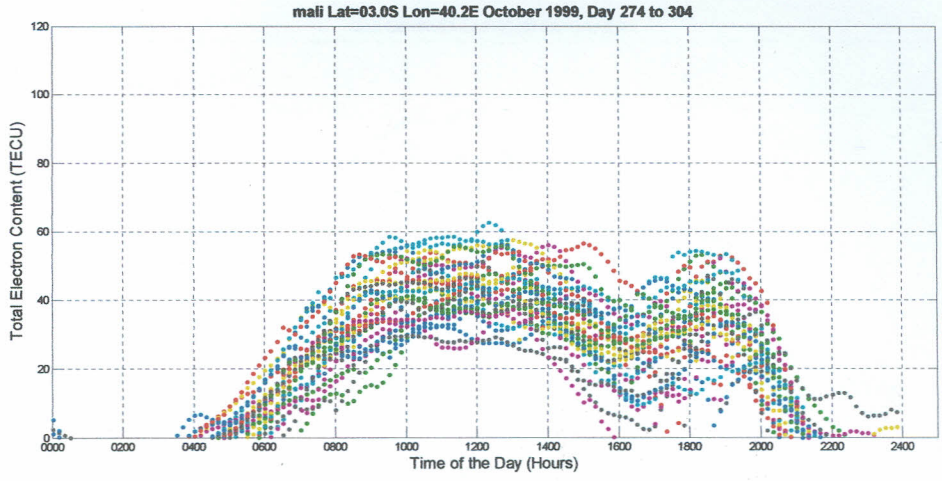

Figure 18: Monthly mass plots of the diurnal variation of TEC for Malindi Kenya for October 1999

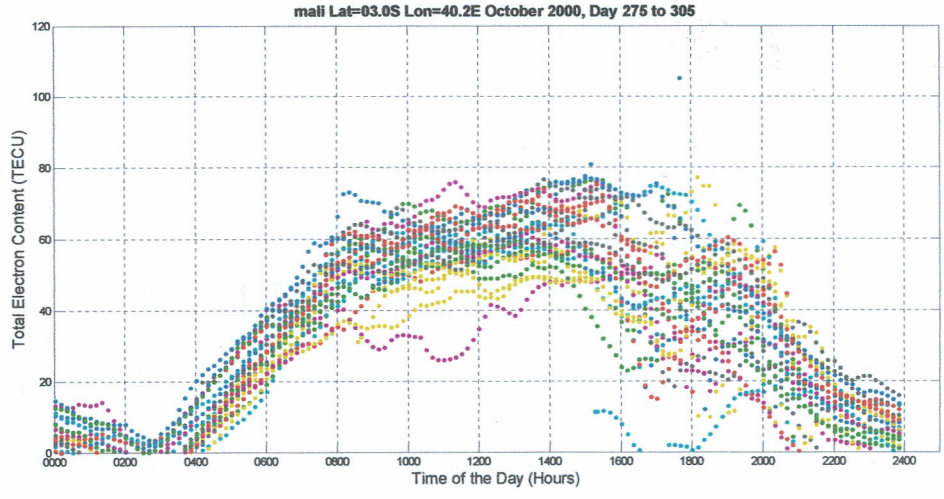

Figure 19: Monthly mass plots of the diurnal variation of TEC for Malindi Kenya for October 2000

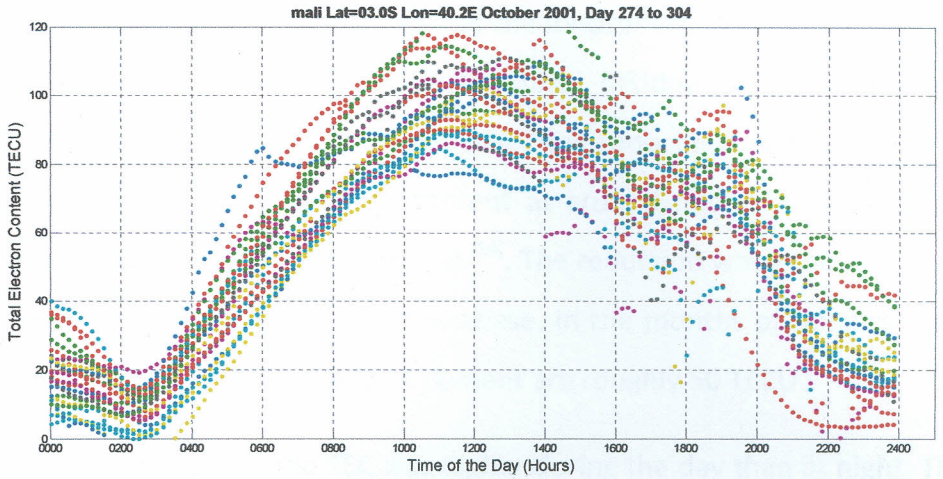

Figure 20: Monthly mass plots of the diurnal variation of TEC for Malindi Kenya for October 2001

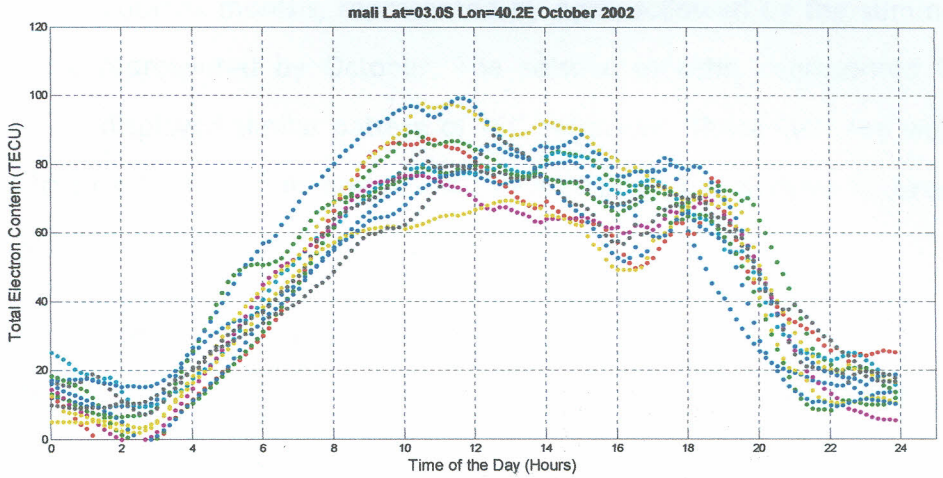

Figure 21: Monthly mass plots of the diurnal variation of TEC for Malindi Kenya for October 2002

From these plots it was evident that the TEC values somewhat increase after sunset and this could be attributed to pre-reversal enhancement.

4.1.1 Diurnal Variation

The observations made from the data plotted in figures 6 to 21 indicated that in all cases the TEC increased rapidly after the local sunrise to reach the daily maxima at around 1100 hours Coordinated Universal Time (UTC) which is also 1400 hour Local Time (LT). Kenyan LT is 3 hours ahead of the UTC. The electron content then started reducing as the afternoon and hence evening and night set in. This happened because as the day progressed from the local midnight, the solar activities increased

causing the ionization in the D, E and F layers of the ionosphere. The enhanced solar radiation in turn increased the TEC. After the local midday or thereabout the intensity of the solar radiation started reducing thus reducing the level of solar activity to attain the minimum electron content at around midnight. This was in agreement with the findings of Rama Rao et al.[14]. The reduction was generally more gradual than the earlier parts of the days' increase. In the months of January 1999 and 2000, the daily maxima of the electron content are roughly 60 TECU.

From the data, it was clear that the TEC was higher during the day than at night. The maximum value could vary from one day to another. The maximum TEC observed was in the March equinox months, represented by April, followed by the summer equinox months, represented by October. The solstice months, represented by January and June, displayed similar pattern of TEC behaviour. These facts too were derived from figure 6 to 21. The minimum value of the TEC was in all cases observed just after 0200 UTC or just before 0300 UTC.

4.2 Results from the interquartile range

The plots of the interquartile range at interval of two hours are shown hereafter in figures 22 to 35.

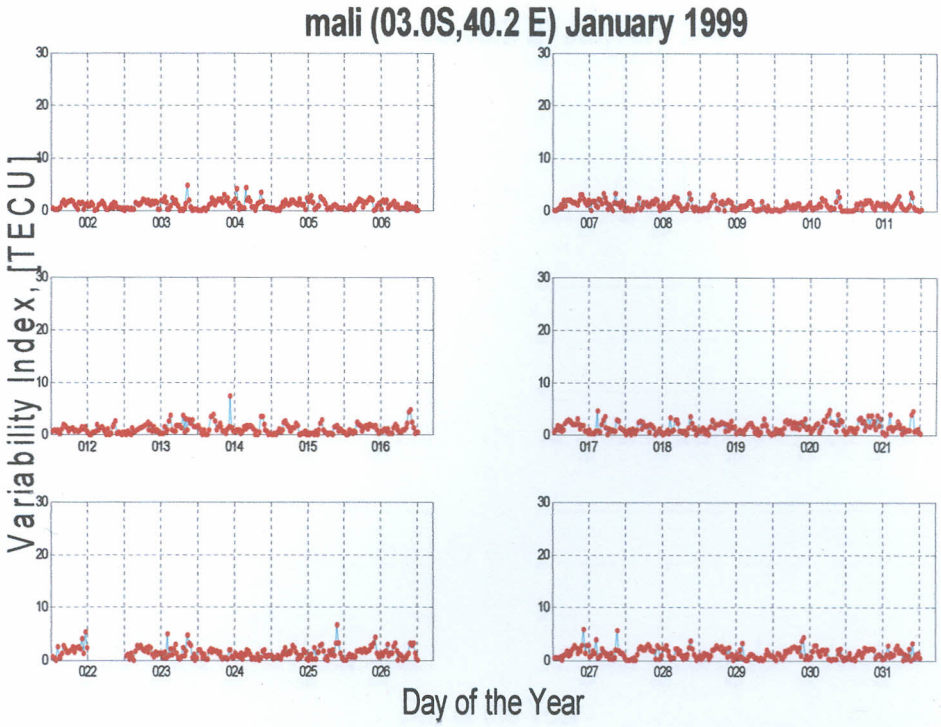

Figure 22: The graph of the interquartile range taken at Interval of Two Hours for Malindi Kenya, mali Lat=03.0S Lon=40.2E, against Day of the Year for January 1999

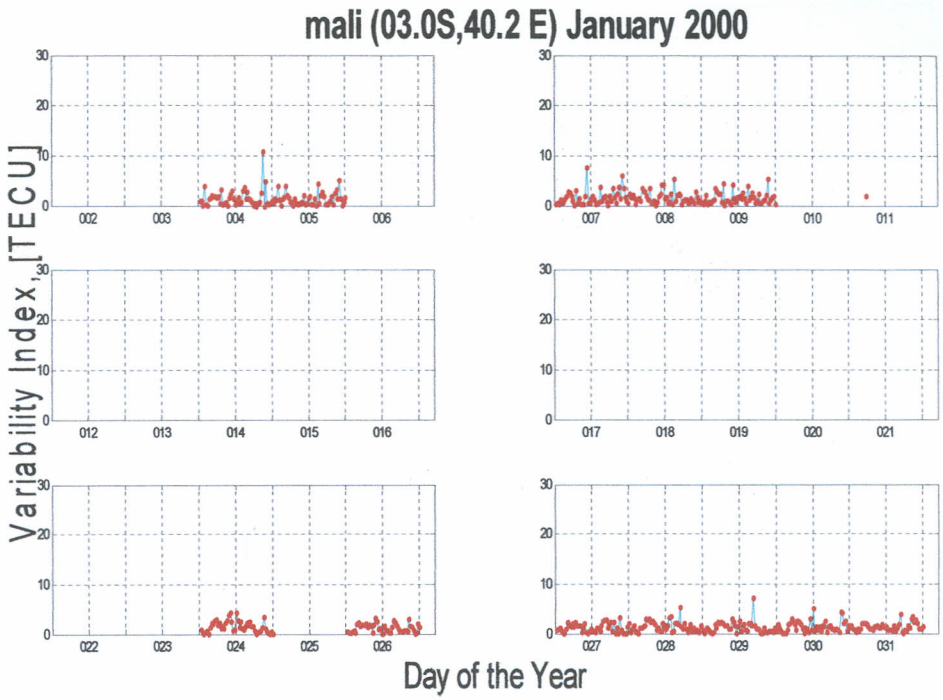

Figure 23: The graph of the interquartile range taken at Interval of Two Hours for Malindi Kenya, mali Lat=03.0S Lon=40.2E, against Day of the Year for January 2000

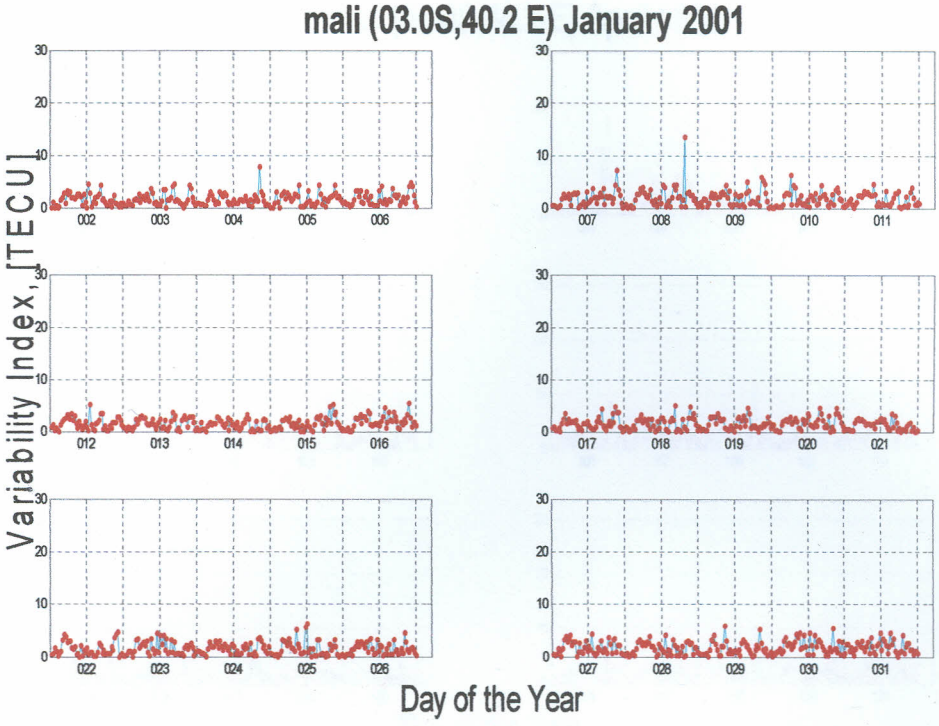

Figure 24: The graph of the interquartile range taken at Interval of Two Hours for Malindi Kenya, mali Lat=03.0S Lon=40.2E, against Day of the Year for January 2001

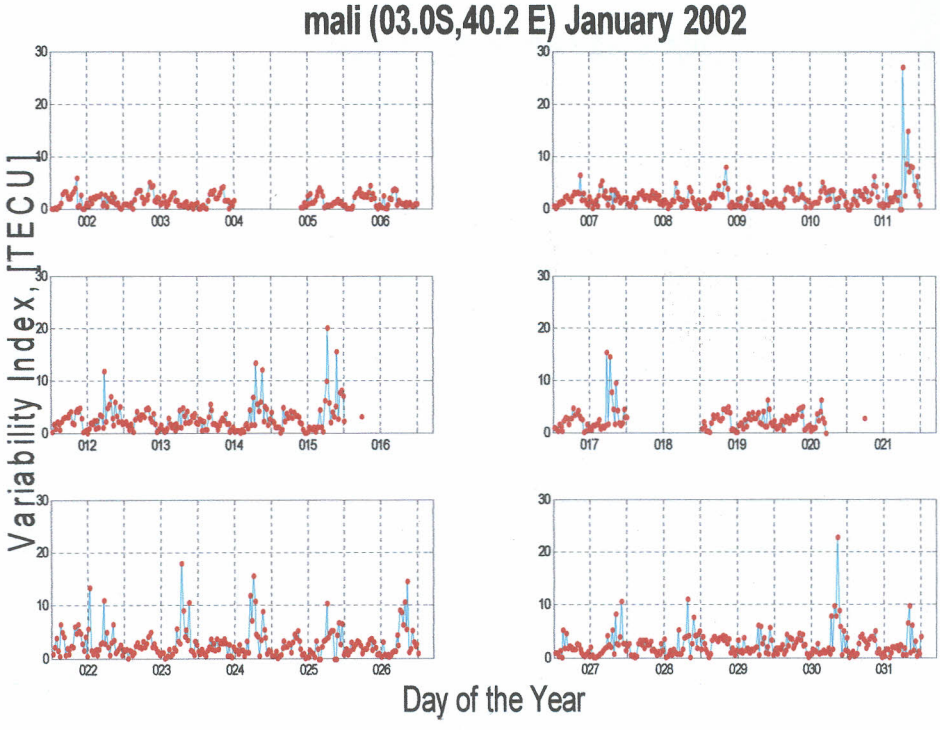

Figure 25: The graph of the interquartile range taken at Interval of Two Hours for Malindi Kenya, mali Lat=03.0S Lon=40.2E, against Day of the Year for January 2002

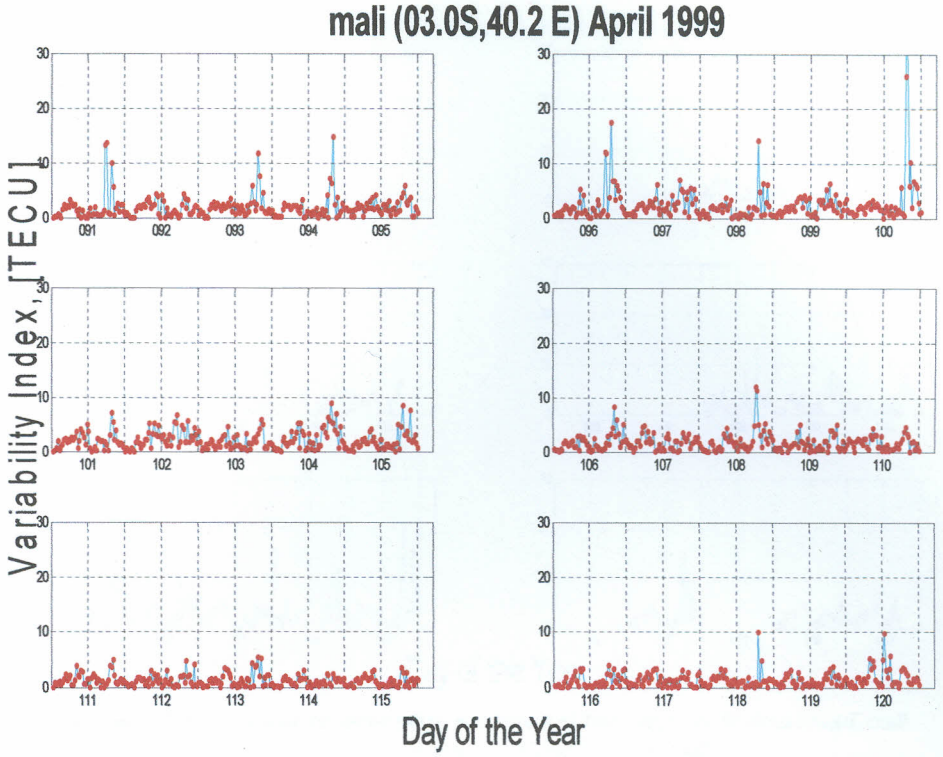

Figure 26: The graph of the interquartile range taken at Interval of Two Hours for Malindi Kenya, mali Lat=03.0S Lon=40.2E, against Day of the Year for April 1999

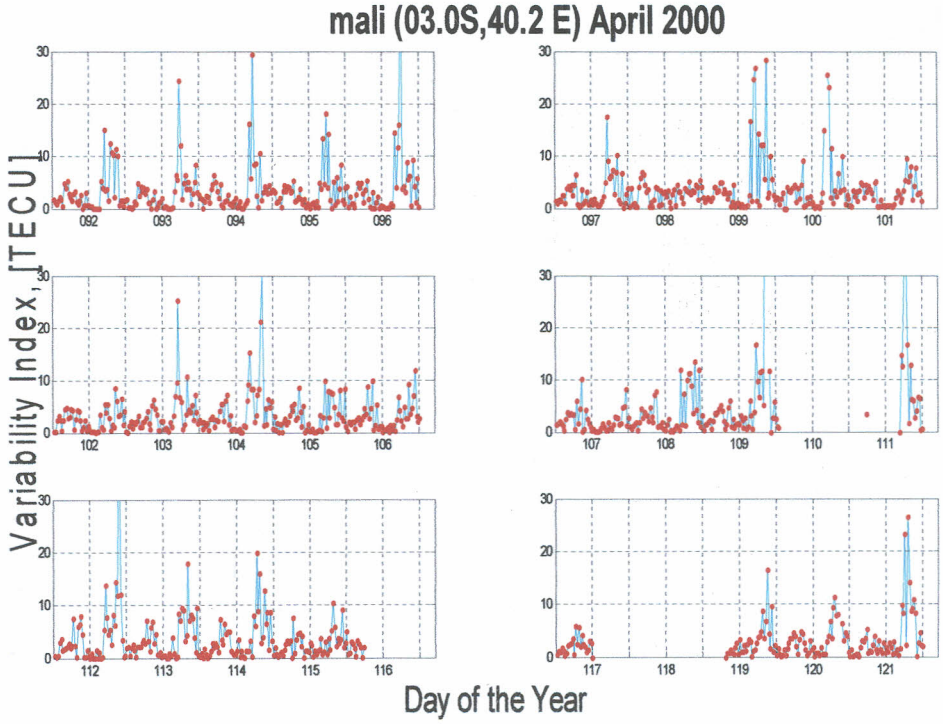

Figure 27: The graph of the interquartile range taken at Interval of Two Hours for Malindi Kenya, mali Lat=03.0S Lon=40.2E, against Day of the Year for April 2000

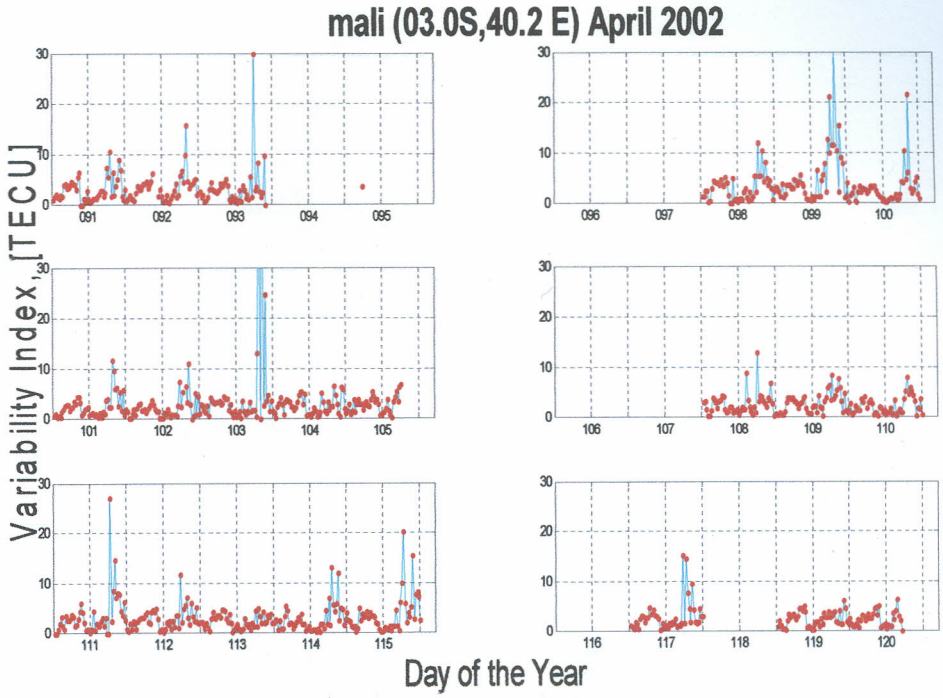

Figure 28: The graph of the interquartile range taken at Interval of Two Hours for Malindi Kenya, mali Lat=03.0S Lon=40.2E, against Day of the Year for April 2002

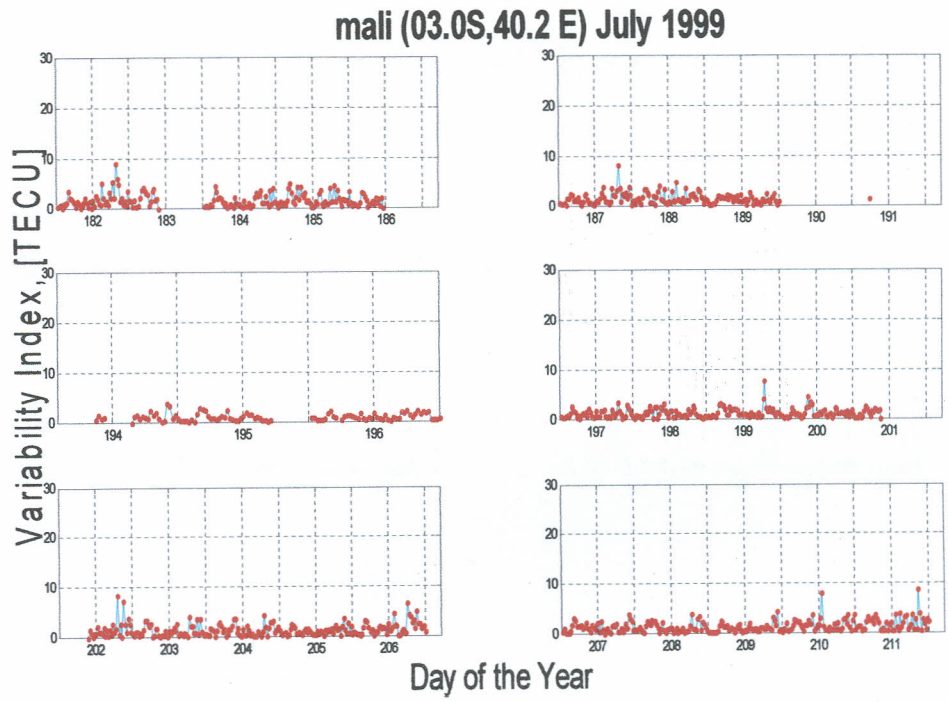

Figure 29: The graph of the interquartile range taken at Interval of Two Hours for Malindi Kenya, mali Lat=03.0S Lon=40.2E, against Day of the Year for July 1999

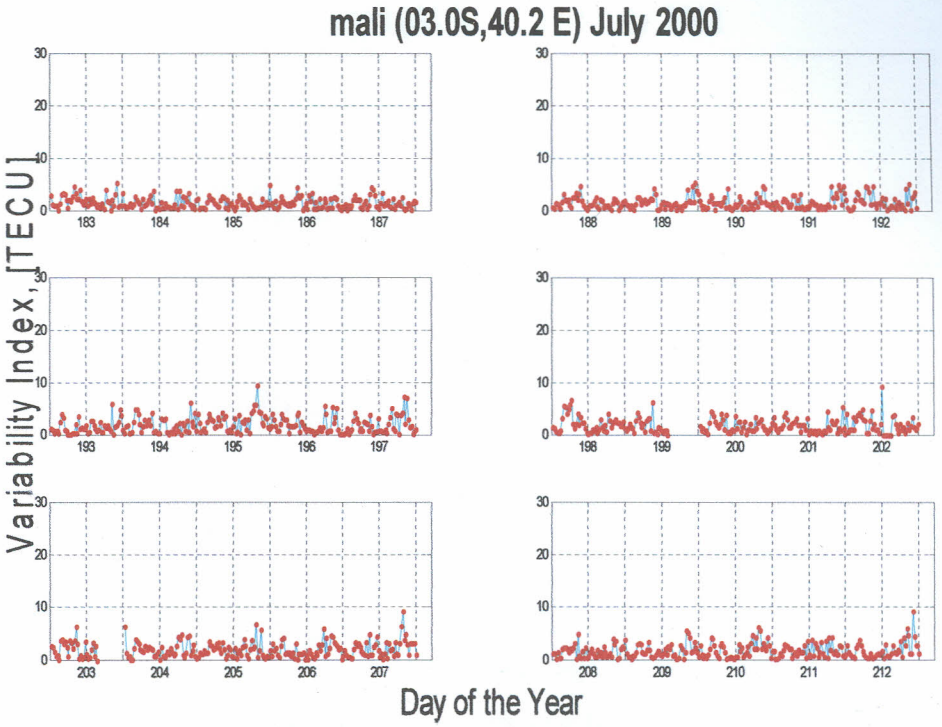

Figure 30: The graph of the interquartile range taken at Interval of Two Hours for Malindi Kenya, mali Lat=03.0S Lon=40.2E, against Day of the Year for July 2000

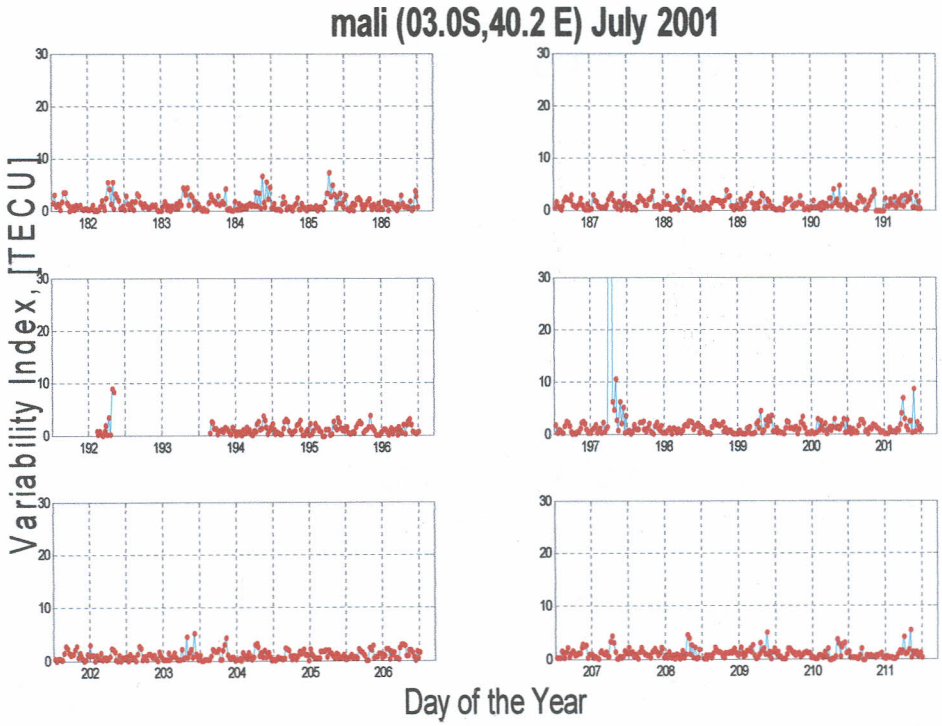

Figure 31: The graph of the interquartile range taken at Interval of Two Hours for Malindi Kenya, mali Lat=03.0S Lon=40.2E, against Day of the Year for July 2001

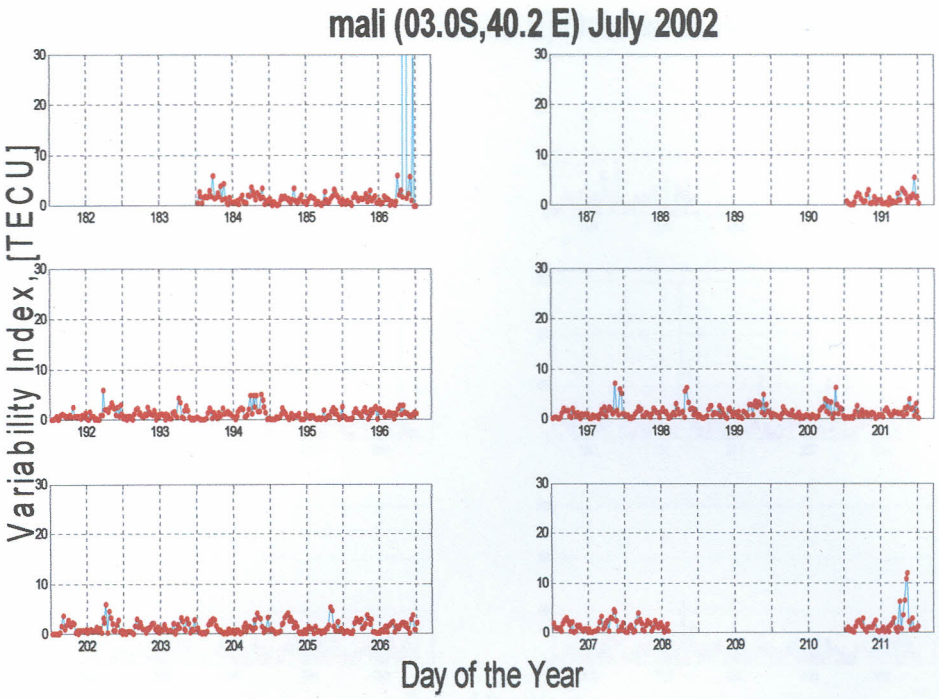

Figure 32: The graph of the interquartile range taken at Interval of Two Hours for Malindi Kenya, mali Lat=03.0S Lon=40.2E, against Day of the Year for July 2002

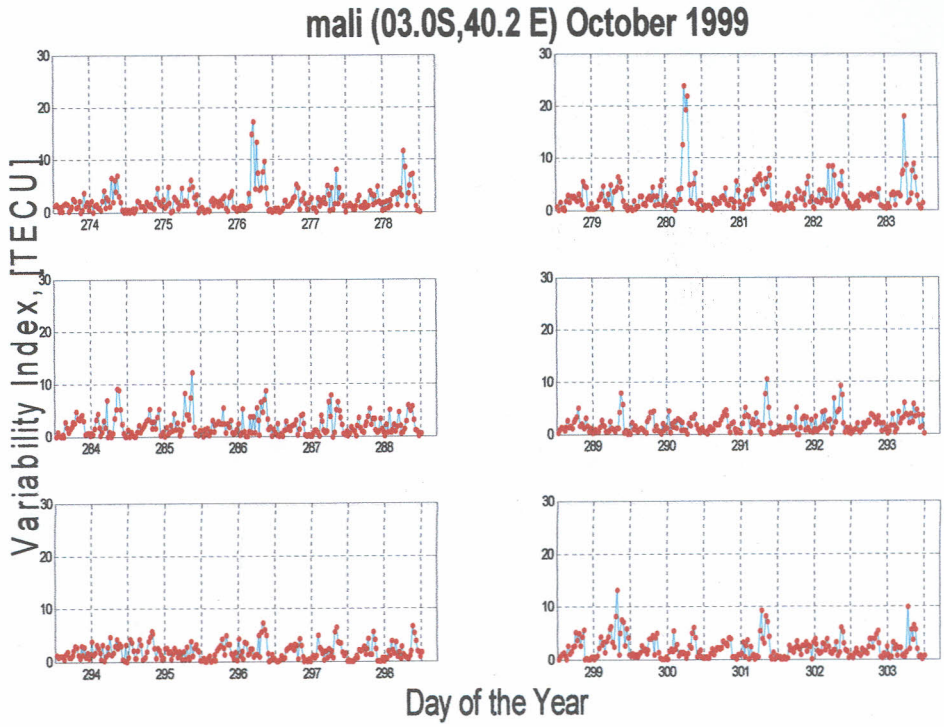

Figure 33: The graph of the interquartile range taken at Interval of Two Hours for Malindi Kenya, mali Lat=03.0S Lon=40.2E, against Day of the Year for October 1999

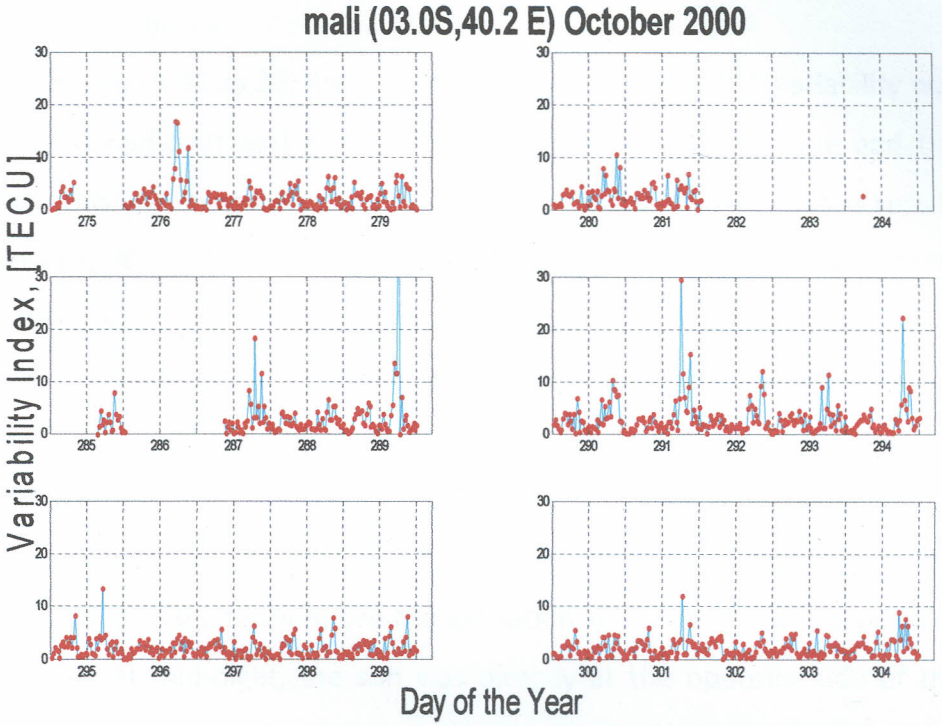

Figure 34: The graph of the interquartile range taken at Interval of Two Hours for Malindi Kenya, mali Lat=03.0S Lon=40.2E, against Day of the Year for October 2000

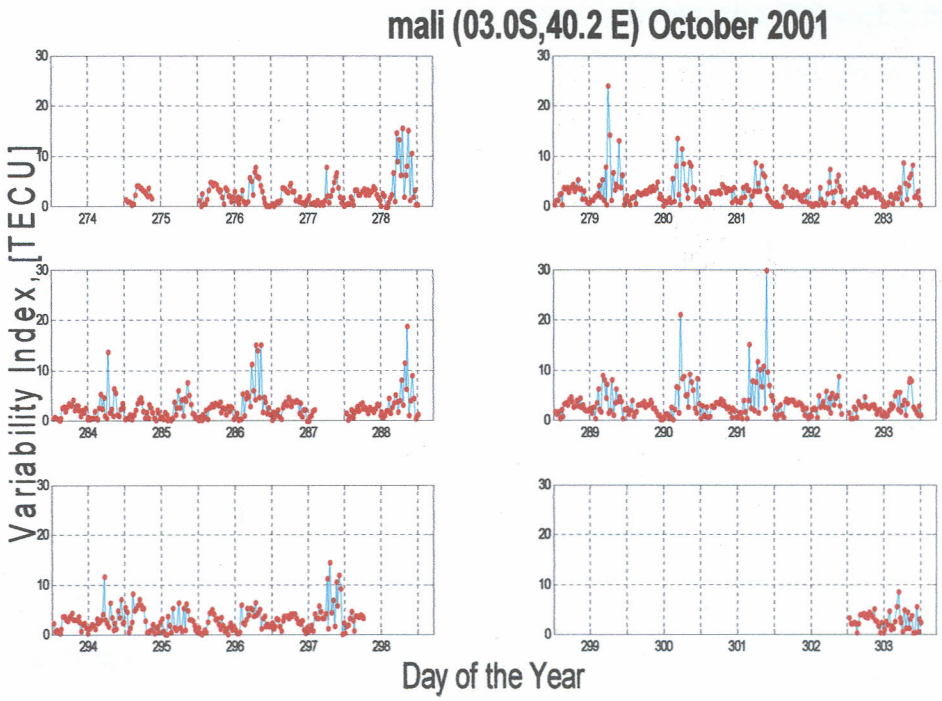

Figure 35: The graph of the interquartile range taken at Interval of Two Hours for Malindi Kenya, mali Lat=03.0S Lon=40.2E, against Day of the Year for October 2001

4.2.1 Diurnal Variability

From the plots in figures 22 to 35, it was evident that the diurnal TEC variability was lowest during the mid-days and mid-nights and highest in the evening and the morning hours. This was in contrast to the findings of the diurnal variations results displayed in figures 70 to 84 in the Appendix IV. The variability of the TEC is different from variation of the same. The major gridlines on the axis of day of the year were placed at the mid-day marks while minor gridlines (in between the calibrations) were indicating the mid-night points. Remarkable TEC variability was noted at around dusk and early morning hours. The reasons for the findings were that during the mid-day, the ionization level had stabilized and so the TEC variability was greatly reduced. The sun was directly overhead and therefore the ionization was almost at the maximum at around midday. At mid-night, the sun was directly at the opposite side of the globe. At that time therefore, the ionization was minimum. At that time also, there was neither ionization nor reconnection of the charged particles. In the evenings, the TEC variability was highest due to the reconnection of the charged particles following the reduced solar radiation. Similarly, during the morning hours, the TEC variability was high since that was the time of ionization occasioned by the solar radiations.

4.2.2 Premidnight Enhanced TEC Variability

Enhanced TEC variability was observed at around 11.00 p.m. local time. Figure 22 displayed that behaviour which was consistent throughout the entire period of study. The enhancement in variability was thought to be caused by the North South neutral wind.

The electric field may result from changes in the ionospheric dynamo processes due to changes in the ionospheric conductivities (electron density) by combined storm effects of the direct penetration and disturbance dynamo electric fields or neutral composition perturbation. Neutral wind and composition effects are also capable of producing the EIA variations during magnetic storms. The neutral wind and composition effects often result as an asymmetric response of the EIA[44].

4.2.3 Seasonal Variability

The TEC variability was further altered by the change of the seasons of the year. From the interquartile range plots in figures 22 to 25, we discovered that the months representing the December Solstice season were generally quiet with minimal variability of TEC in the early hours of each day and evening hours. It was found that the maximum TEC variability was found to be at around 1100 hour and 2300 hours LT. The daily maximum TEC variability indices hardly reached 5 TECU and only exceeded this value in very few cases. The quietness of the season was because during the December solstice, the sun was in the farthest south relative to the equator and the length of time between Sunrise and Sunset was very short. This greatly inhibited the solar activities and hence the reduced the TEC variability. More so, there was no ionospheric storm, which could perturb the ionosphere. The levels of TEC variability in the evenings during the month were found to be higher than the levels during the morning hours of the day. This was true in almost all cases but was particularly clearer is some seasons as can be seen in figure 25 representing December solstice of the year 2002 than others. During that season it was observed that between 0800 hours and 1000 hours LT when we also have high TEC variability; the variability indices averagely reached 5 TECU while between 2200 hours LT and 2400 hours LT, the variability indices in several cases were above 10 TECU.

The TEC variability of all the months representing the March equinox season under study was generally higher than that of the months representing the December Solstice season, i.e. January. During the March equinox, the sun crossed the Equator moving northward. There was therefore intense solar radiation, which was evident by the high variability of the TEC. The months of March equinox therefore saw the variability of the TEC reaching as high as 25 TECU, as could be observed in figure 27.

The month of April 1999 showed the variability indices higher than the average of those of the months of December Solstice season under study by just a few units. The other months of March equinox recorded higher variability indices than 5 TECU. The variability indices of the month of April 1999 were in many cases going beyond 4

TECU with the highest values reaching 10 TECU. The highest TEC variability of each day in any case was observed between around 2200 hours and 2400 hours LT.

The month of March equinox season with highest TEC variability was that of 2000 with the maximum variability index going up to 100 TECU as could be seen in day 099 of the year. This was the case because during the year, the solar activity was going to the maximum. During the June solstice season, or June solstice the sun is farthest north and the length of time between sunrise and sunset is the longest of the year. The bulk of the solar radiation is shifted towards the northern hemisphere leaving the equatorial region with reduced activity. For that matter, the variability index hardly went beyond 10 TECU. The average variability index could be put at around 5 TECU.

The June solstice represented by July and December solstice represented by January, months had very similar characteristics. They were generally found to be quiet with minimal and normal TEC variability in the early morning hours, late afternoon, and evening hours. The maximum TEC variability was found to be at around 1100 hour and 2300 hours LT. The daily maximum variability indices ranged between 2 TECU and 5 TECU. The same was the case during the entire four years under study.

During the September equinox season, the sun crosses the equator moving southward. This brings intense ionization around the equatorial region. It can be comparable to the ionization during the March equinox when the sun has just crossed the equator towards the northern hemisphere.

The variability of the TEC in during the March equinox was nearly similar to that of the months of the October equinox. The latter was however less intense than the former. This was deduced by comparing figures 26, 27 and 28 with figures 33, 34 and 35. Normally the TEC variability during the two months should be similar. Kenya lies at the southern crest of the equatorial anomaly and therefore this caused the difference.

4.2.4 Variability Due to Solar Cycle

Annual variability of the TEC along the equatorial region was evident. There was variability caused by the solar cycles, which took eleven years. See Appendix I and II for the 11 years solar variability according to the plots obtained from the website of the Solar Influences Data Analysis Center (SIDC), which is the solar physics research department of the Royal Observatory of Belgium. The SIDC includes the World Data Center for the sunspot index and the ISES Regional Warning Center Brussels for space weather forecasting[47].

The day-to-day variability of the months of December solstice, represented by January in this research, was observed over the years. In the year 1999, the maximum variability indices hardly exceeded 10 TECU, save for only a few exceptions. This was evident from figures 22 to 25. The year 2000 was characterized with low percentage of data availability and therefore could not be used to make authoritative conclusions. January 2001 showed 100% data availability. As opposed to the observations made in the December solstice of 1999, during the December solstice of 2001, the variability indices was mostly higher than 4 TECU. This could be because this was the year of solar maximum and therefore was characterized with the highest level of solar activity. In the December solstice of 2002, variability indices showed significantly increase in activities with the interquartile range reaching as high as 10 TECU. This however was not consistent with the expectation given that the 23rd solar maximum occurred around 2000 and therefore needs further research.

It would be interesting to know the trend in 2001. However, because of low data availability, the month representing the December solstice was not considered for analysis. Out of the 30 days, there were only data in five days which translated to just 17%, which cannot give a reliable conclusion.

From the years with good percentage of data availability, the March equinox of 2000 displayed the highest TEC variability. Figures 26 to 28 give elaborate characterization. From the figures, we confirm that 2000 was the year with the highest TEC variability out of the years with high data availability. It was clear that

both the diurnal variation and TEC variability were higher in the year 2001 than 2000.

The information displayed in Appendix III from Kyoto Data Website [28] confirms that there was a major storm between 6th and 7th of April 2000. That information confirmed the finding from this research showing abnormal variability right from the beginning of the months and climaxing in day 99. Day 99 was the 7th of October 2000. The plots from the same data site indicated other sub storms on 2nd, between 3rd and 4th and on 16th of the same month. This happened because the month was during the year or approaching the year of the solar maximum.

The plots from the World Data Center for Geomagnetism, Kyoto also confirmed that. From their data plot in the Appendix III, it was observed that in 2001 alone, there were six major storms as opposed to 2000, which had three. Day 8, 11, 13, 17, 22 and 28 of 2001 all had large storms while in 2000 only day 3, 6 and 16 had large storms.

The March equinox month of 2002 was bogged with low data availability of 73% though could be used to make some inference. The variability index was averagely at 20 TECU and could in some cases reach 30 TECU and beyond. In day 099, the index was 40 TECU. In the year 2002, the solar maximum year had passed and so the variability index was reducing.

July 1999, which represented the June solstice months, had the peak variability indices as the least as compared to similar months in the four years, 1999, 2000, 2001 and 2002 as can be observed in figures 29 to 32. In very isolated cases, the values of the interquartile range reaching 10 TECU were found. This was comparable to the December solstice season of the same year. This happened because the relative positions of the sun to the earth in the two cases enable the solar activities in the ionosphere to be similar.

Just like in the previous seasons, June solstice season represented by, July, of 2000 saw a remarkably higher variability than June solstice season of 1999. In several

cases, it was observed that the peak values of the variability index exceeded 4 TECU. It was in that year (2000) that the June solstice season saw the maximum values of the variability indices. The June solstice of 2001 and 2002, both had comparably lower TEC variability.

In the beginning of the September equinox represented, by the month of October 1999, the early morning peak of variability index was hardly reaching 5 TECU while the late evening peak of the variability indices was in many cases above 10 TECU. As the month progressed, the values of the morning maxima appreciated while the values of the evening maxima depreciated until the two sets of daily maxima of the variability index leveled at around 9 TECU. The remaining three years had similar trends of the TEC variability.

The sets of the plots, which we analyzed, gave us similar patterns on the ionospheric nature around Malindi and by extension, Kenya. The solar activity as was evident in the nature of variability index. The solar cycle variability climaxed in the year 2001 as was expected, given that it was the year of solar maximum in the eleven-year cycle. This was in tandem with various information obtainable from the space weather and geomagnetic sites. Among such sites were the World Data Center for Geomagnetism, Kyoto, operated by Data Analysis Center for Geomagnetism and Space Magnetism Graduate School of Science, Kyoto University[39] and Solar Influences Data Analysis Center (SIDC)[46], (the latter being the solar physics research department of the Royal Observatory of Belgium), among others.

In each year, we also expected the highest TEC variability during the equinox months and the lowest variability indices during the solstice months. That expectation was also confirmed.

It however turned out that the variability of TEC during the winter and June solstices were not the same. The same was the case with the variability of TEC in winter and the solar equinoxes. They were not exactly similar as was expected. During the March equinox, the level of TEC variability was higher than during the summer

equinox. The TEC variability during December solstice was higher than that during the June solstice. This could be attributed to Appleton anomaly.

The equatorial F region represents an interesting anomaly, usually called the Appleton anomaly or just the equatorial anomaly. On simple theory, as has been indicated earlier in this work, the electron density should be a maximum over the dip equator at the equinox, because the sun is overhead and so the ionization rate is very high. In fact, the electron density falls to a minimum over the magnetic equator and passes through maxima at latitudes 10^{o} or 20^{o} north and south of the equator. The explanation is found in electrodynamic lifting, in which a horizontal electric field, acting in the presence of a horizontal magnetic field, produces a plasma flow in the vertical. The equatorial anomaly can be explained by an electric field of a few microvolts per metre directed towards the east. Given the magnetic field induction of 0.5G (5×10^{-5} Wb m^{-2}) directed south to north, a vertical drift of 10 ms^{-1} is produced. The electric field is thought to arise in the E layer. As the plasma is lifted to greater altitude, it meets field lines that connect to the ionosphere north and south to the equator, down which it may diffuse under gravity. In general, the plasma motion is a combination of electrodynamic drift and thermal diffusion, but the net result is depletion over the equator and concentration at latitudes 10^{o} or 20^{o} from the magnetic equator. The phenomenon has been described as a fountain effect.

4.3 Results Using the Boxplots

To scrutinize the TEC variability in details, the boxplots were used to analyze the nature of the TEC variability. This tool was meant to be the most elaborate means of studying the variability given that each plotting point revealed a lot about the nature of the variability. However, the scale, which we could realistically use to do the plots, did not allow us to realize the full benefits. The boxplots all the same offered invaluable means of verifying the results obtained using the method of interquartile range.

The Figures 36 to 64 are the sets of box plots for the chosen months, January, April, July and October, in the four years, 1999, 2000, 2001 and 2002. Each month's plots are made in two different to enhance the visibility of the plotting points.

Figures 36 and 37 present the TEC variability for the month of January 2000. The month was characterized with outage such that only twelve days had data. That explains why a good portion of the graph is bare. The boxplots were rather short and the maximum median values reaching only a peak of 40 TECU.

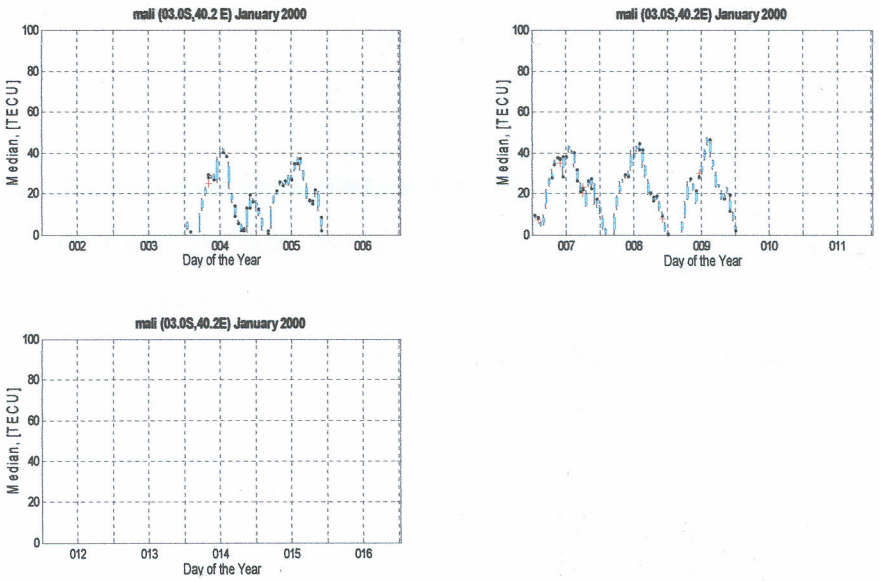

Figure 36: Box plots showing interquartile Range [Lat=03.0S Lon=40.2E], Part One of January 2000

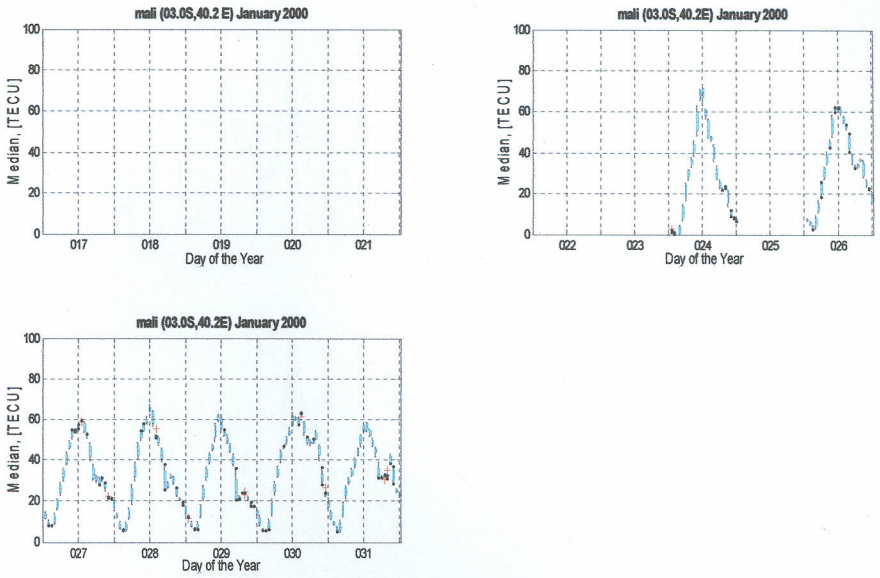

Figure 37: Box plots showing interquartile Range [Lat=03.0S Lon=40.2E], Part Two of January 2000

Figure 38 and 39 were the plots showing the variability during the month of January 2001. The data availability was perfect. The sizes of the boxes in the plots were in many cases bigger than in the previous case. This indicated increased variability of the TEC as the day of the solar maximum is approached.

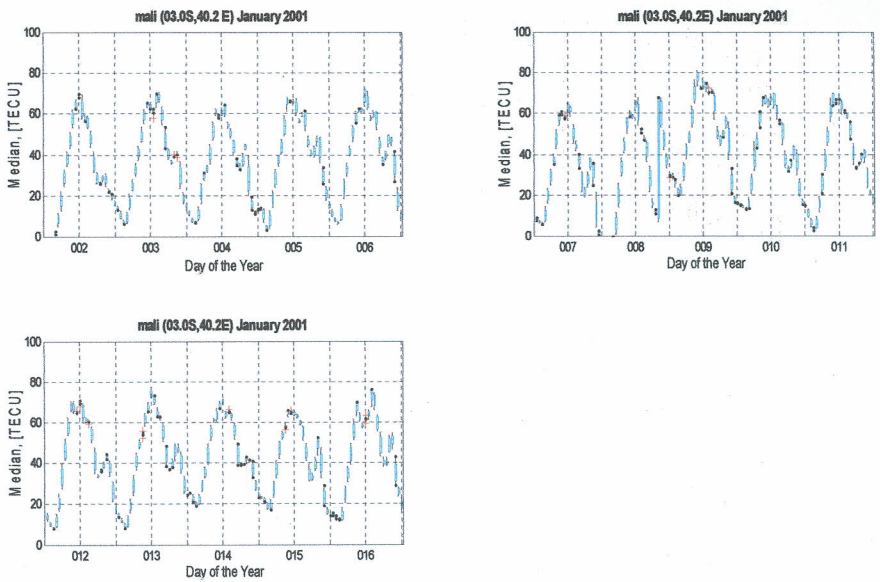

Figure 38: Box plots showing interquartile Range [Lat=03.0S Lon=40.2E], Part One of January 2001

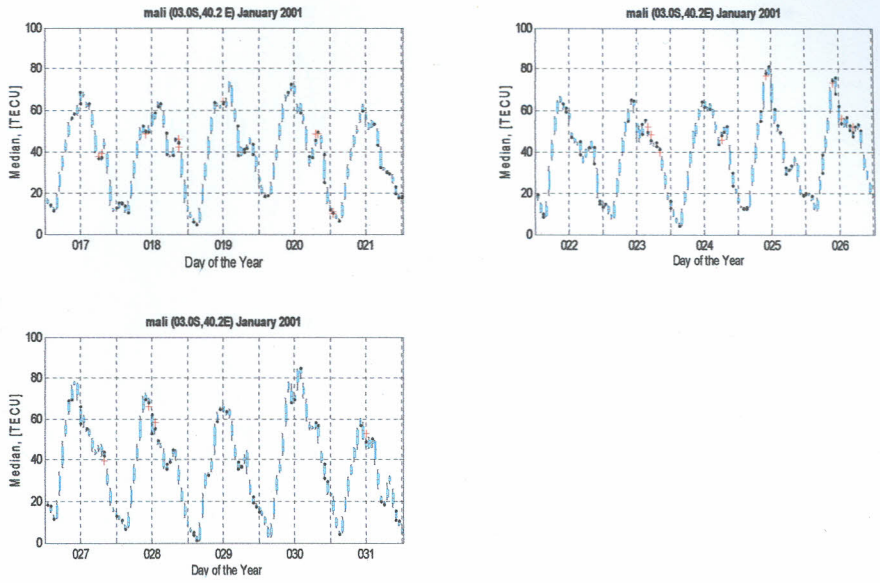

Figure 39: Box plots showing interquartile Range [Lat=03.0S Lon=40.2E], Part Two of January 2001

Figure 40 and 41 shows the variability in January 2002. The general variation of TEC as demonstrated by the maximum TECU reached was higher than all the other cases considered. However, the sizes of the box plots, which are the actual measure of the TEC variability, are slightly reduced.

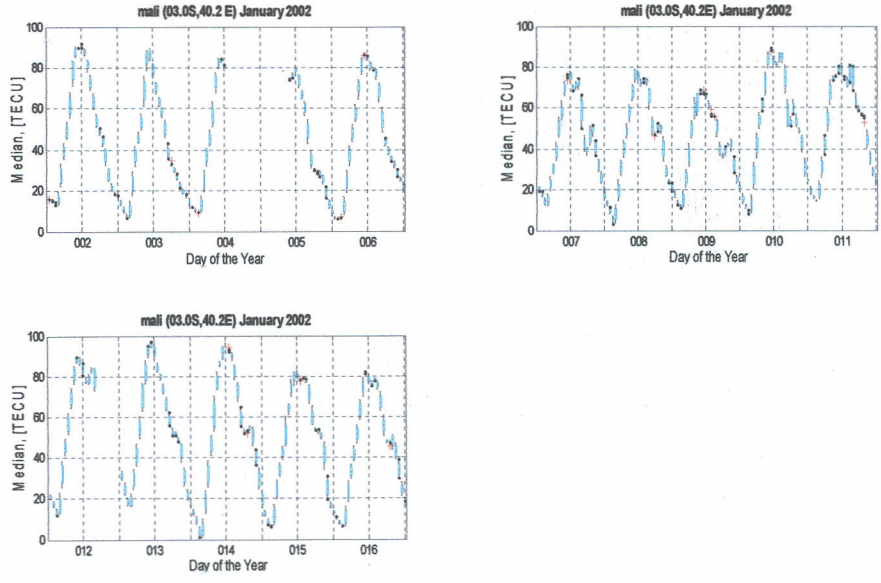

Figure 40: Box plots showing interquartile Range [Lat=03.0S Lon=40.2E], Part One of January 2002

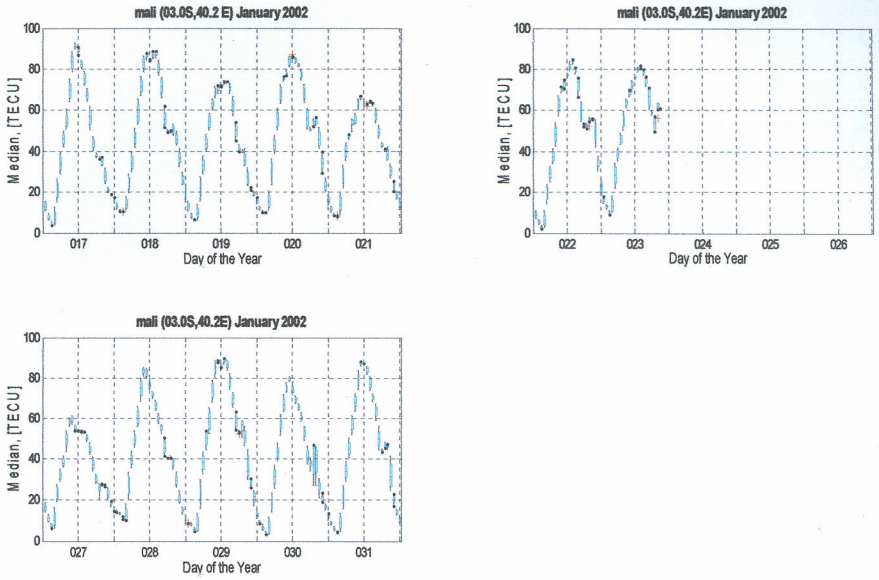

Figure 41: Box plots showing interquartile Range [Lat=03.0S Lon=40.2E], Part Two of January 2002

Figures 42 and 43 illustrate the variations and the variability of the TEC in the month of April 1999. The TEC variability is fairly low but higher than the previous months of January. The maximum value of the TEC reached is however high, 80 TECU.

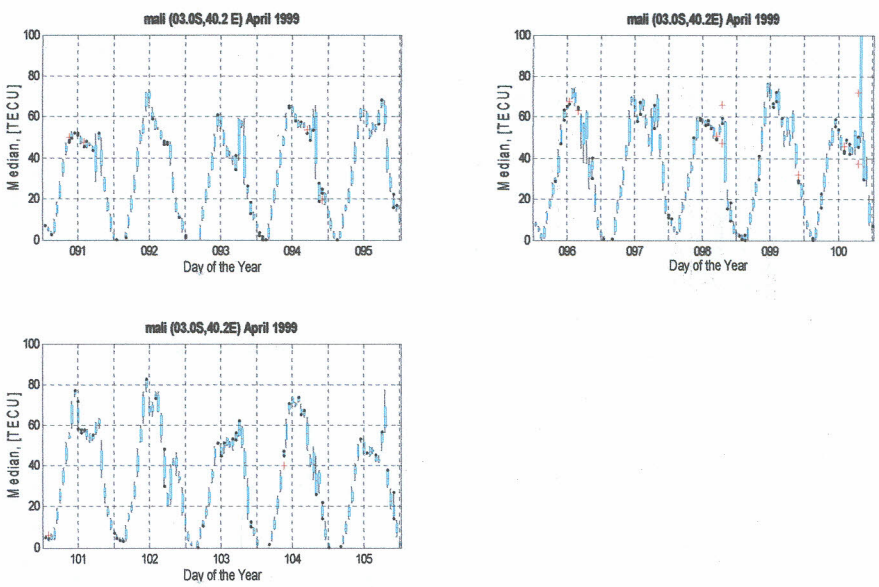

Figure 42: Box plots showing interquartile Range [Lat=03.0S Lon=40.2E], Part One of April 1999

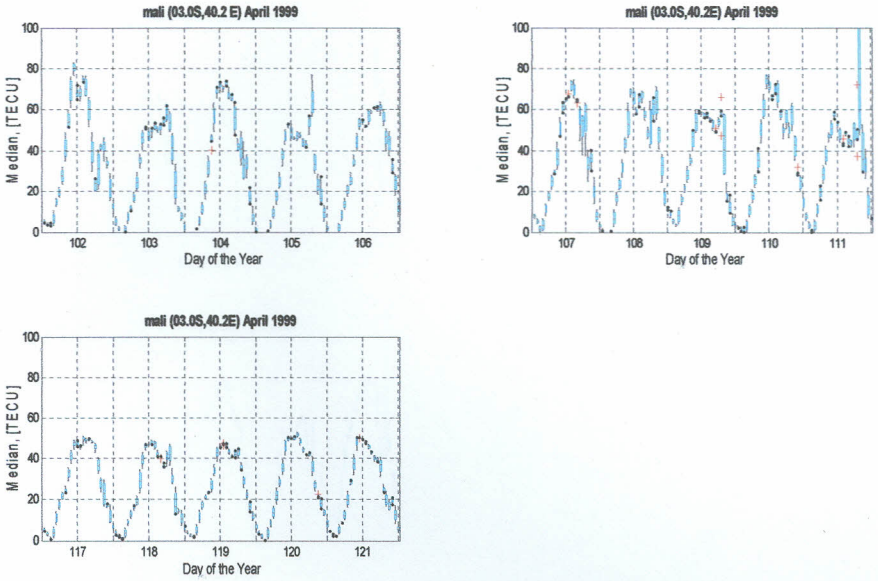

Figure 43: Box plots showing interquartile Range [Lat=03.0S Lon=40.2E], Part Two of April 1999

Figure 44 and 45 showed significant enhancement in the TEC variability. The maximum TEC reached was 100 TECU. The data availability was about 75%.

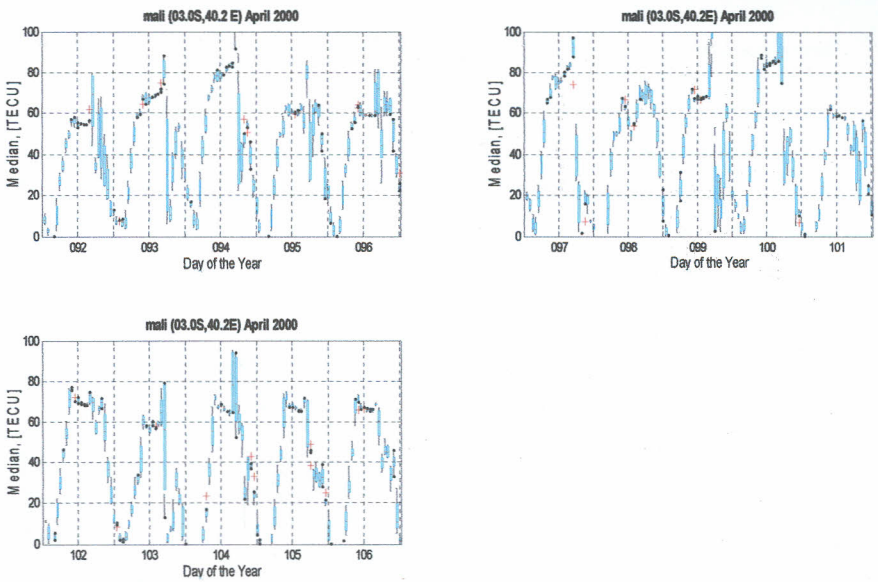

Figure 44: Box plots showing interquartile Range [Lat=03.0S Lon=40.2E], Part One of April 2000

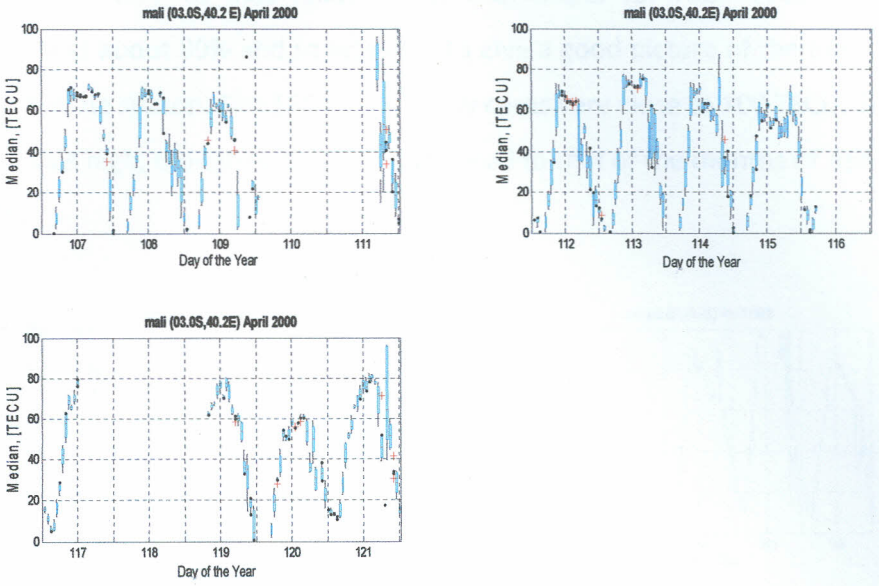

Figure 45: Box plots showing interquartile Range [Lat=03.0S Lon=40.2E], Part Two of April 2000

Figure 46 presented the findings of April 2001. The data availability was the entire month was less than 25%, which was low. Like in figure 36 and 37, the unplotted parts indicated data gaps. From the few days, the TEC was at all time high, more or less 100 TECU.

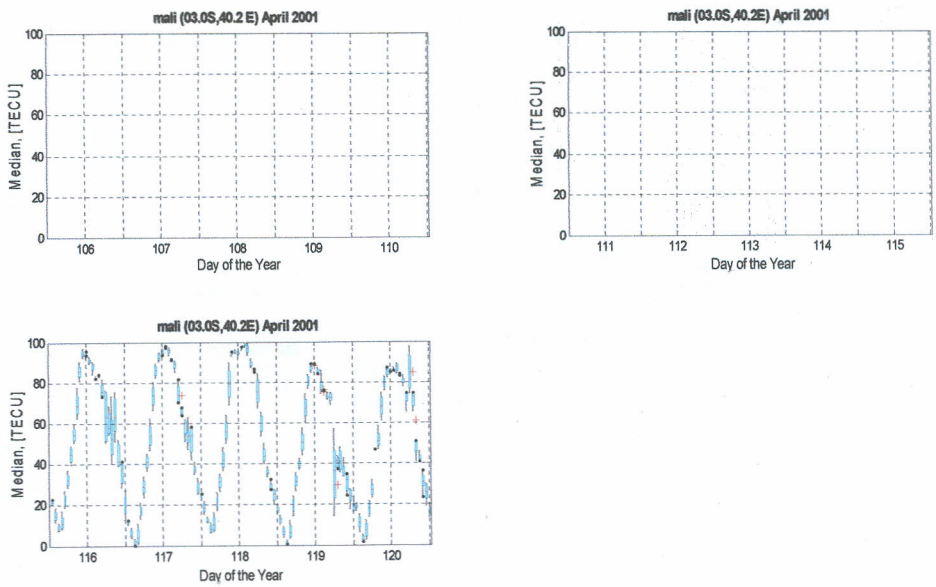

Figure 46: Box plots showing interquartile Range [Lat=03.0S Lon=40.2E], Part Two of April 2001

The figures 47 and 48 that follow show the results for April 2002. The data availability was about 80% and so was able to give a good picture of the ionospheric condition for the season. The TEC was in many cases very close to 100 TECU. The TEC variability was high, though reduced as compared to that of the months of April 2000 and 2001.

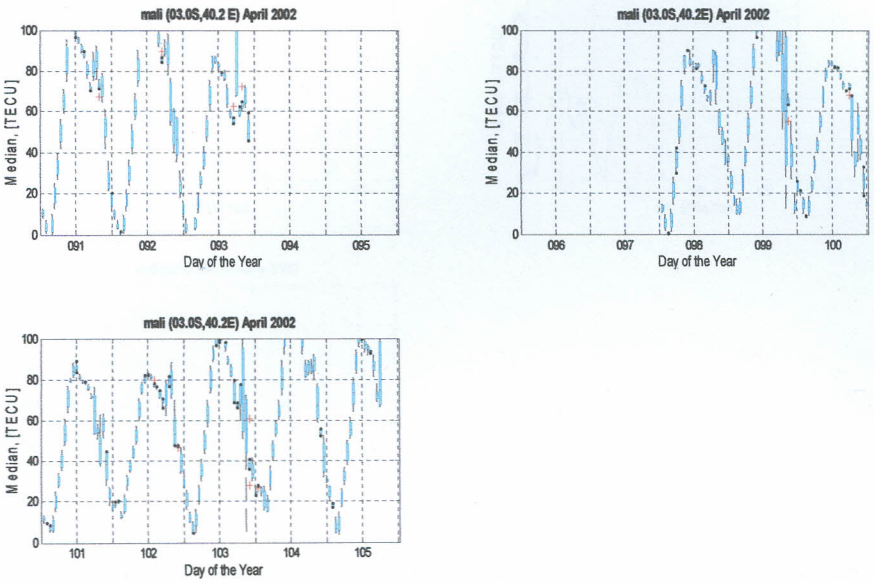

Figure 47: Box plots showing interquartile Range [Lat=03.0S Lon=40.2E], Part One of April 2002

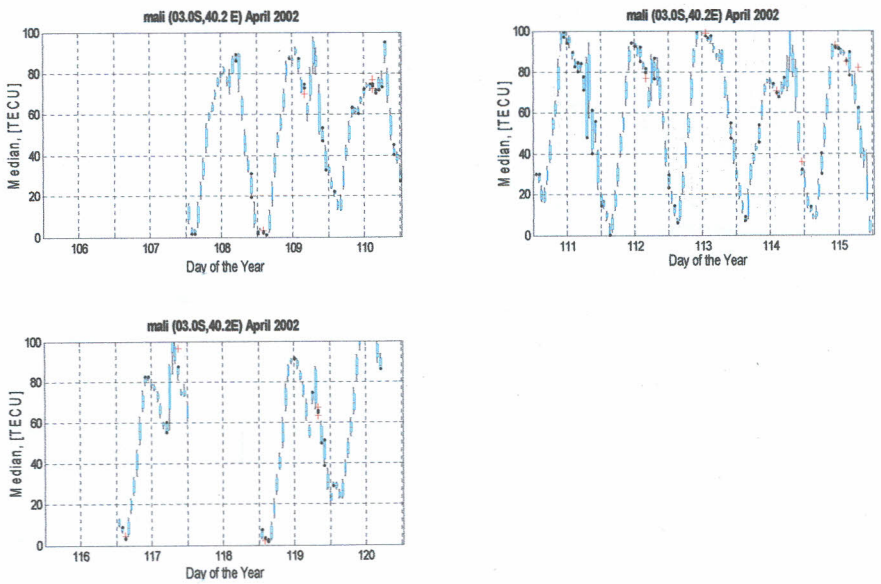

Figure 48: Box plots showing interquartile Range [Lat=03.0S Lon=40.2E], Part Two of April 2002

The month of July 1999 illustrated experienced very low values of TEC. The maximum value, which was slightly above 60 TECU, was observed in day 185. There was also good data availability. The TEC variability was however very low as demonstrated by the sizes of the boxes.

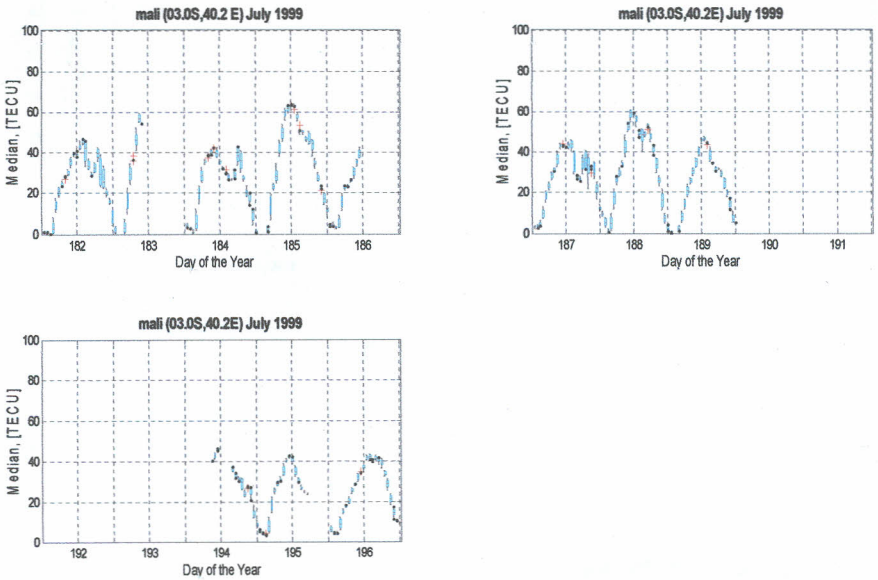

Figure 49: Box plots showing interquartile Range [Lat=03.0S Lon=40.2E], Part One of July 1999

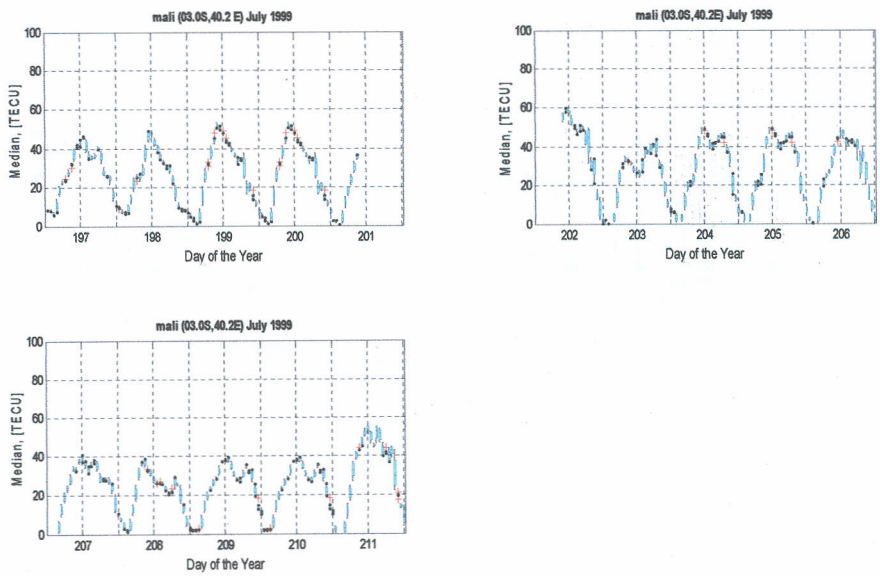

Figure 50: Box plots showing interquartile Range [Lat=03.0S Lon=40.2E], Part Two of July 1999

July 2000 illustrated in figures 51 and 52 experienced good data availability. The TEC was higher than that of July 1999, with the values reaching about 70 TECU. The TEC variability was however very low, from the sizes of the boxes.

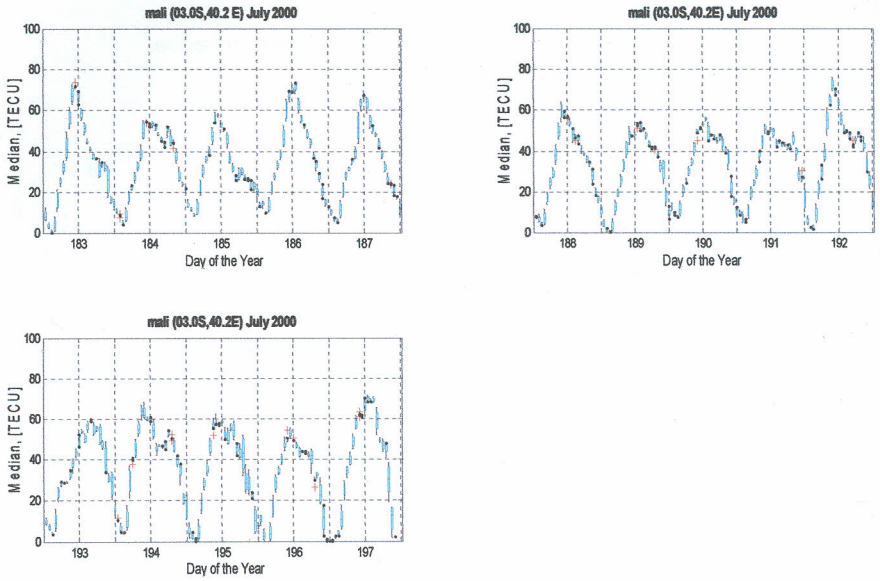

Figure 51: Box plots showing interquartile Range [Lat=03.0S Lon=40.2E], Part One of July 2000

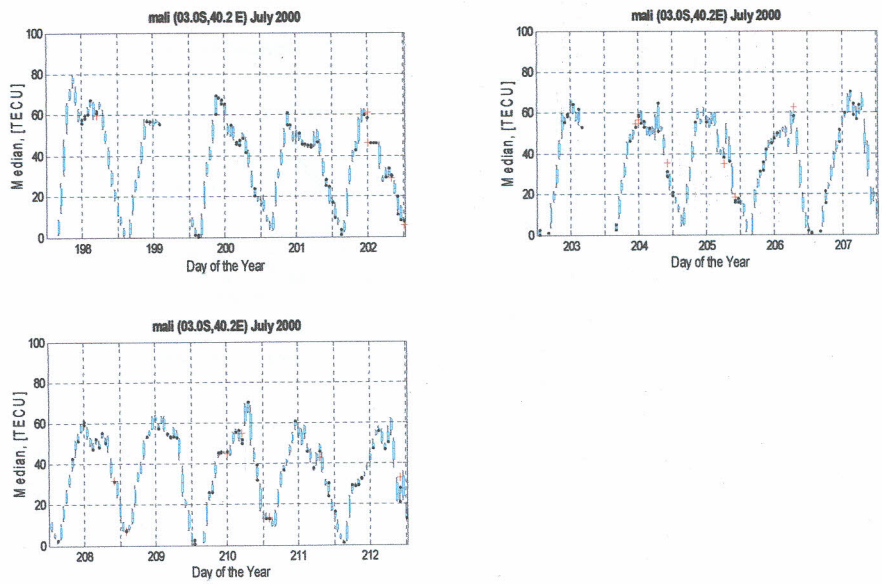

Figure 52: Box plots showing interquartile Range [Lat=03.0S Lon=40.2E], Part Two of July 2000

Figures 53 and 54 show the boxplots for July 2001. The values of the TEC reached about 80 TECU. A slight improvement in the variability was observed as compared to July 2000.

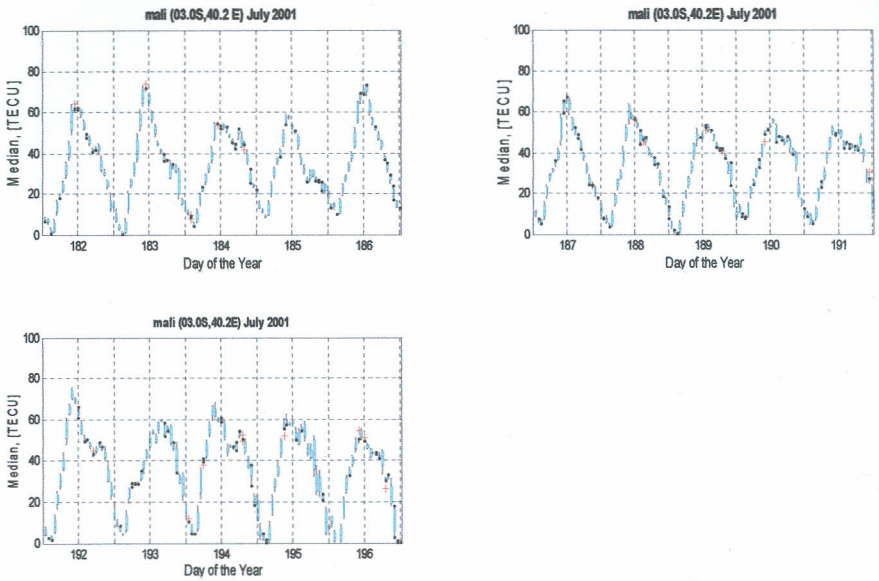

Figure 53: Box plots showing interquartile Range [Lat=03.0S Lon=40.2E], Part One of July 2001

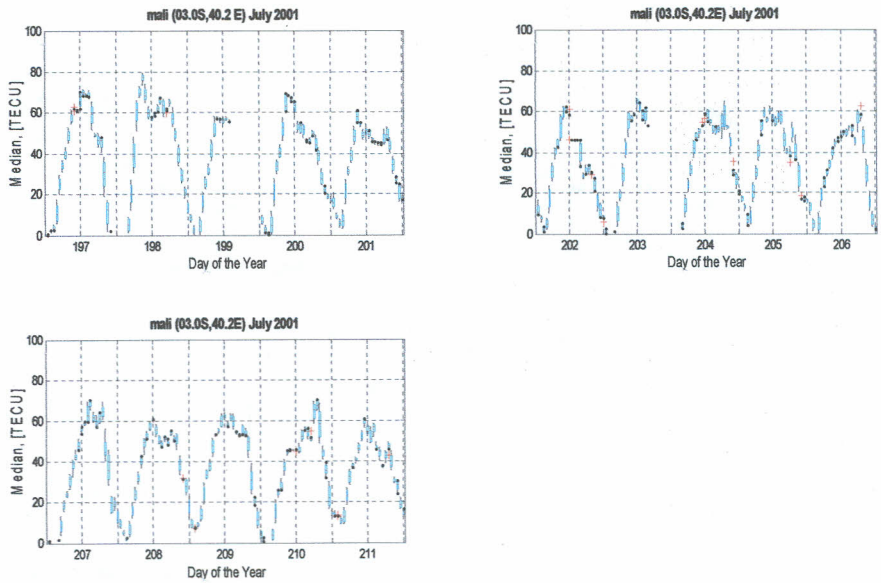

Figure 54: Box plots showing interquartile Range [Lat=03.0S Lon=40.2E], Part One of July 2001

Figure 55 and 56 shows the TEC variability in the month of July 2002. The data availability was about 50% which was not good. The maximum TEC reached was roughly 50 TECU. The sizes of the boxes were also small showing low TEC variability.

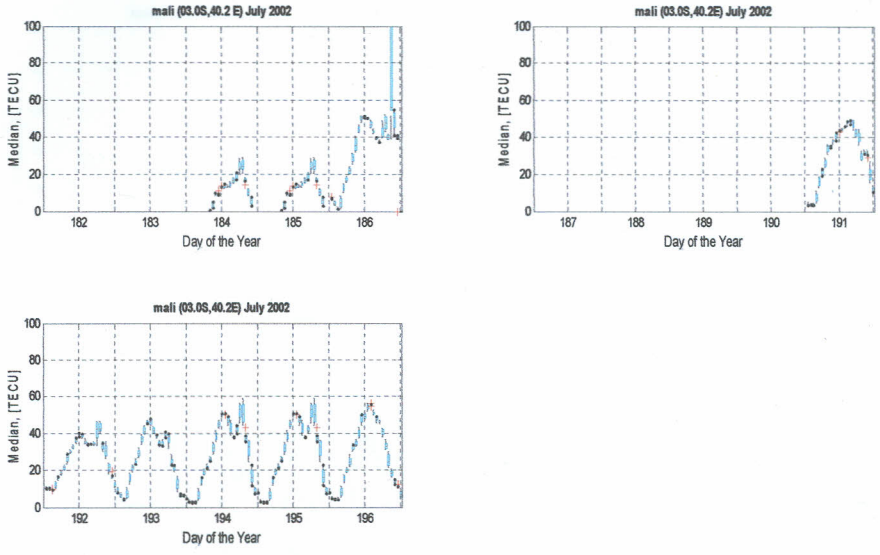

Figure 55: Box plots showing interquartile Range [Lat=03.0S Lon=40.2E], Part One of July 2002

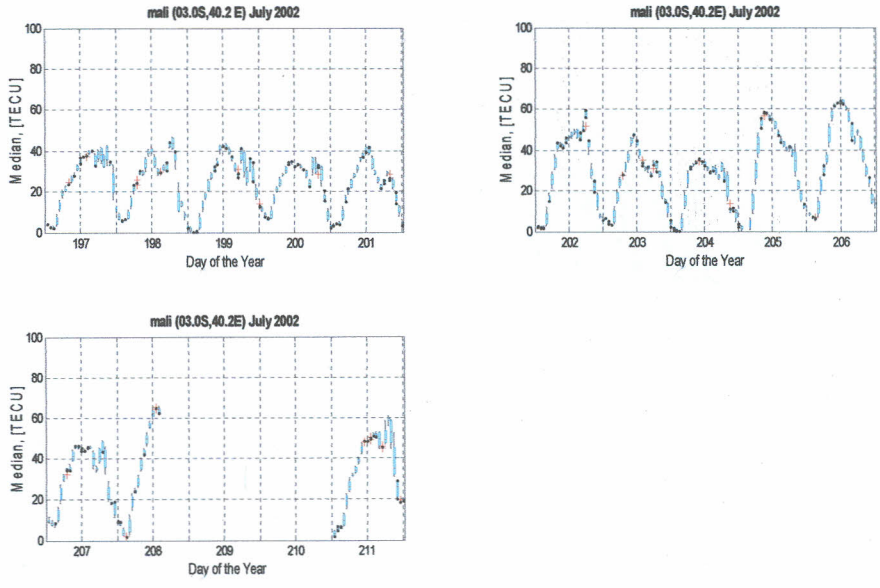

Figure 56: Box plots showing interquartile Range [Lat=03.0S Lon=40.2E], Part Two of July 2002

Figure 57 and 58 show the TEC variability in the month of October 1999. The data availability was good and the maximum TEC value reached during the period was 60 TECU. The variability of the TEC from the size of the boxes was moderate.

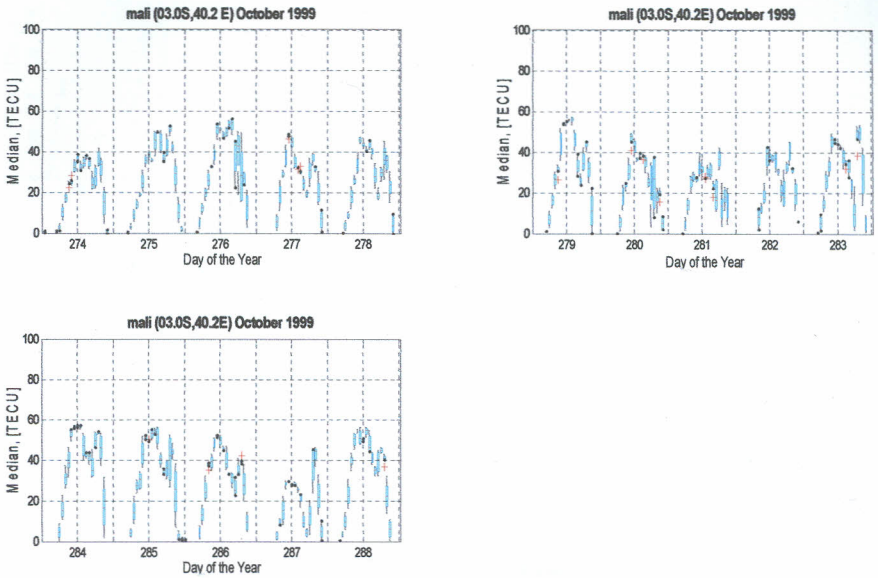

Figure 57: Box plots showing interquartile Range [Lat=03.0S Lon=40.2E], Part Oneof October 1999

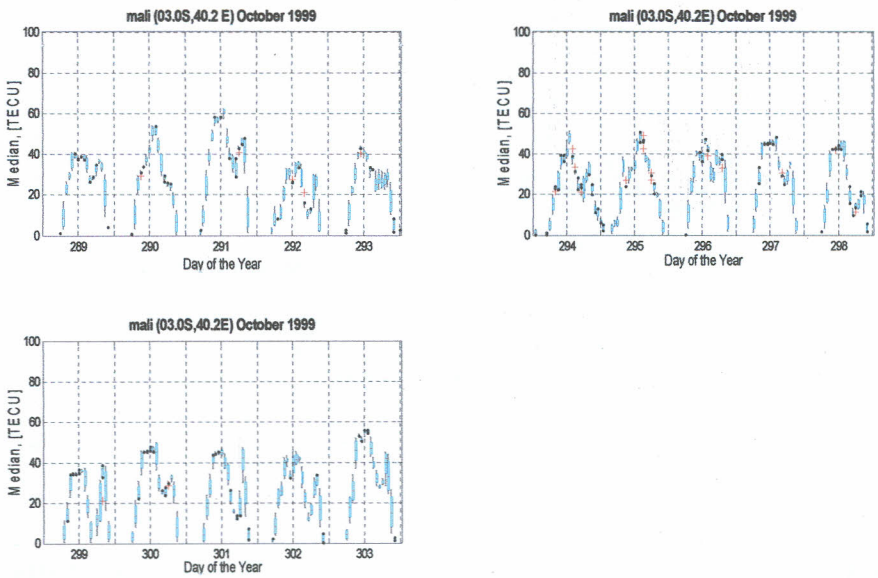

Figure 58: Box plots showing interquartile Range [Lat=03.0S Lon=40.2E], Part Two of October 1999

Figure 59 and 60 are the variability boxplots for October 2000. The maximum TEC is 80 TECU. The TEC variability is fairly large—from the sizes of the boxes.

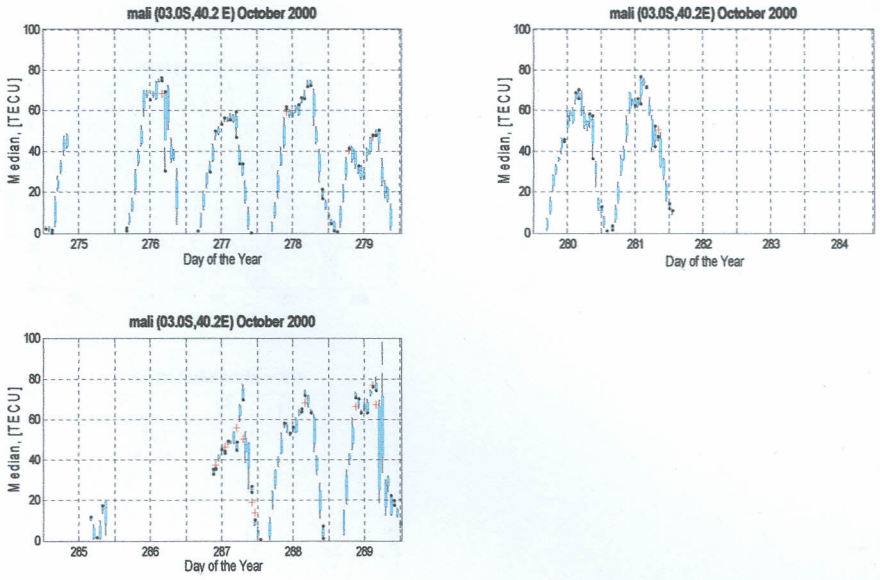

Figure 59: Box plots showing interquartile Range [Lat=03.0S Lon=40.2E], Part One of October 2000

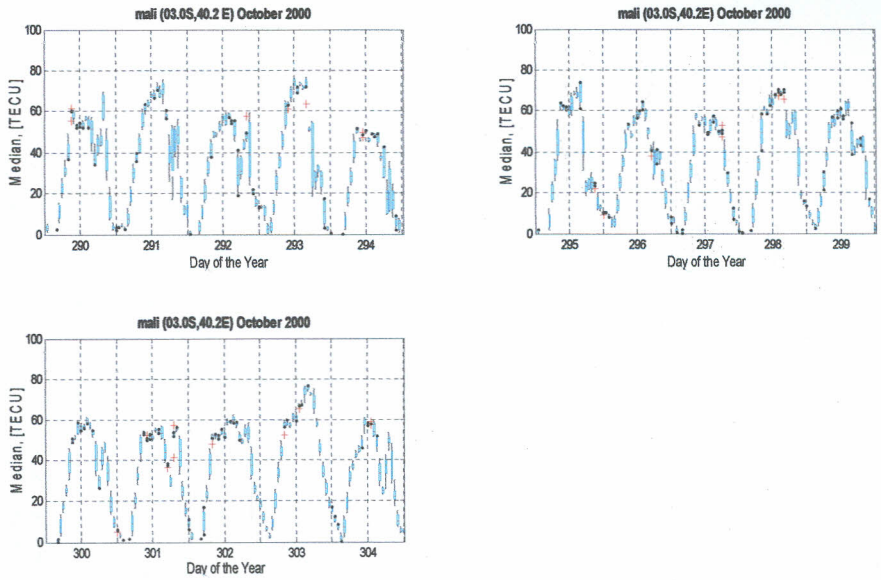

Figure 60: Box plots showing interquartile Range [Lat=03.0S Lon=40.2E], Part Two of October 2000

Figure 61 and 62 presents the variability plots for October 2001. The TEC is all times high, in many case 100 TECU. The boxplots also showed enhanced variability, much higher than what was observed in January and July.

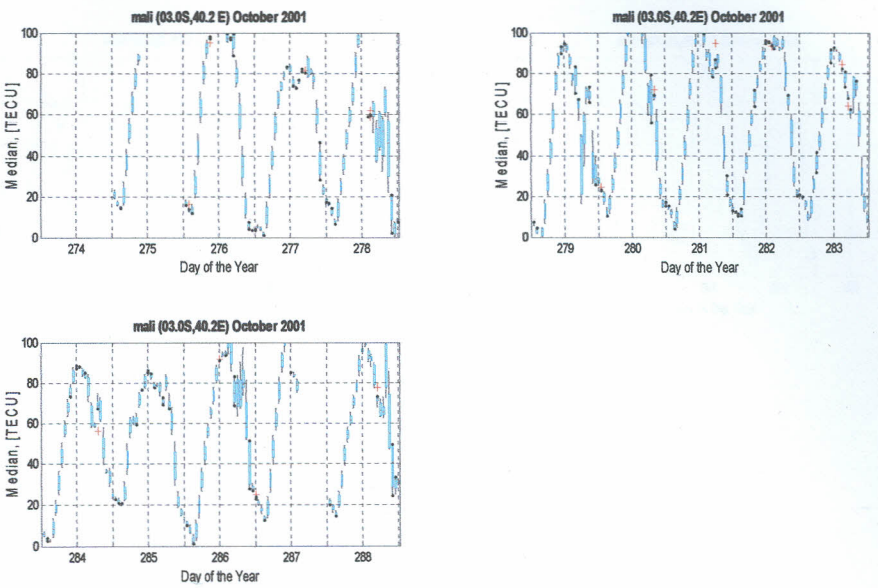

Figure 61: Box plots showing interquartile Range [Lat=03.0S Lon=40.2E], Part One of October 2001

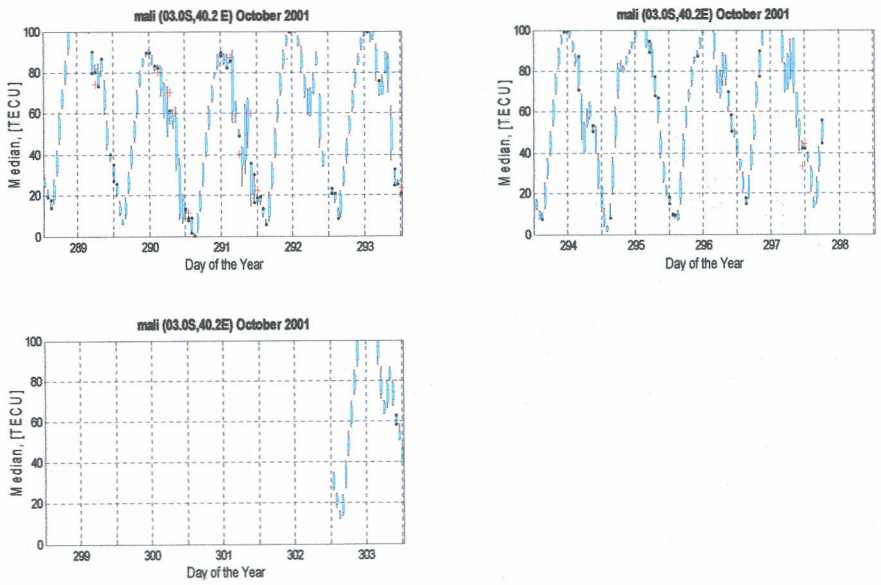

Figure 62: Box plots showing interquartile Range [Lat=03.0S Lon=40.2E], Part Two of October 2001

The variability in the month of October, hereafter presented in figure 63 and 64, displayer low data availability. Variability was greatly reduced. However, the TEC was still high as compared to October 2001.

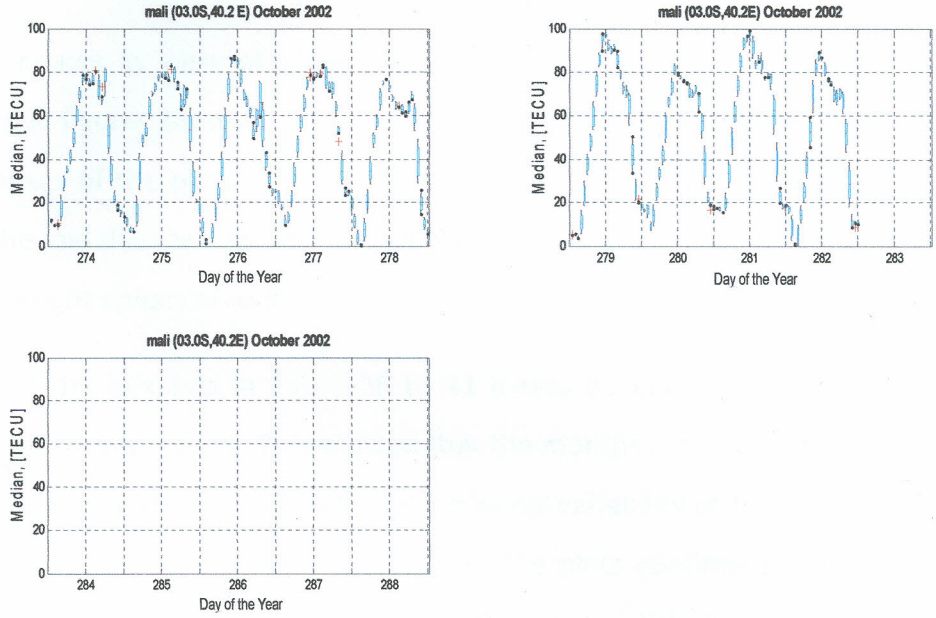

Figure 63: Box plots showing interquartile Range [Lat=03.0S Lon=40.2E], Part One of October 2002

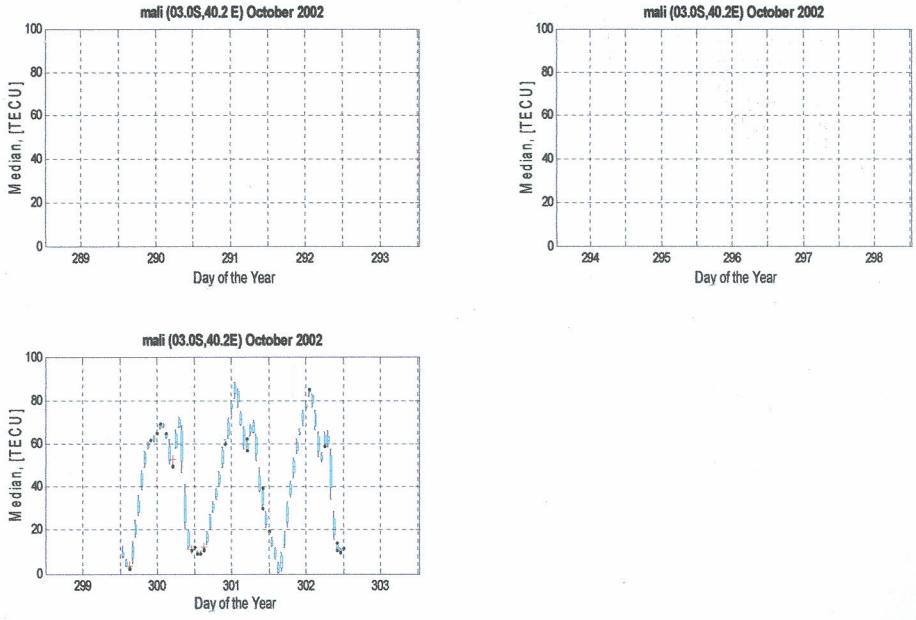

Figure 64: Box plots showing interquartile Range [Lat=03.0S Lon=40.2E], Part Two of October 2002

4.3.1: Discussion from the boxplots

The variations of the median points in the boxplots depicted diurnal variation. The TEC increased as the day progressed to reach the daily maxima at around 1400 hours LT. the pattern was observed to be consistent throughout the period under study.

Similar findings as were obtained about the diurnal variability from the boxplots displayed in figures 36 to 64. In those figures, it was observed that the length of each of the boxes of the plots was maximum in the mornings and evening but shortest during the mid days and around mid nights. Figure 36 clearly showed the occurrence of premidnight enhancement.

Looking at the boxplots in figure 36 to 41 it was observed that the boxes in the plotting points were short. This showed that the months representing the December Solstice season were generally quiet with minimal variability of TEC in the early hours of each day and evening hours. The rest of the plots confirmed the seasonal and solar cycle variability as was observed using the interquartile range plots.

CHAPTER FIVE

5.0 Conclusion and Recommendations for Future Work

5.1 Conclusion

From the research, it was clear that there were diurnal, monthly and seasonal TEC variability during the period, 1999 to 2002. Remarkable diurnal variability of the TEC was noted at around dusk and early morning hours. The morning high was as a result of ionization caused by the increased solar radiation. The dusk high TEC variability was because of the reconnection of the charged particles caused by the reducing solar radiation. Low TEC variability was observed near the midnight and midday. This was always the case for Malindi during the entire period covered by the research. This means that the amount of TEC in the ionosphere could be more easily predicted during the midday and midnight than any other time of the day. There was observed an enhanced TEC variability just before midnight, a pattern which was observed in all the months. The enhancement was caused by the North South neutral winds.

The variability of the TEC depends on the position of the sun relative to the equator. During equinoxes, there is higher variability of TEC than during solstices. It was also noted that the TEC variability during the March equinoxes followed by summer equinoxes, under study were generally higher than that of all the other seasons. The summer equinoxes had the least TEC variability followed by the March equinoxes. The difference in the TEC variability in the two sets of seasons could be attributed to Appleton or equatorial anomaly.

The TEC variability patterns over the years kept on changing. Generally, the TEC variability in 2000 and 2001 were the highest in the four years. During the solar maximum period in the eleven-year solar cycle 23, it was expected that the year 2001 had the highest TEC variability. However there was no data for April 2001, but the highest TEC variability was observed during the month of April 2000 for the entire period. This was most likely due to a series of solar storms occasioned by the high solar radiaton. The research findings gave us what was to be expected around

the time of other solar maxima as well that would come in future. We expected a repeat of the pattern between the year 2010 and 2013 being the next period of the maximum in the eleven years solar cycle 24.

5.2 Recommendations for Future Work

To develop a more complete morphology of the TEC variability for the equatorial region, it is important that a future study consider up to 12 to 15 years spread of data from the same station or from any other station in Kenya. This will be good enough to cover one solar cycle along the equatorial region. A study using data for a longer period than 15 years can also be considered if the data can be found. Data availability for such a long period has been a major challenge in Africa.

It is also important that a similar study be carried out using more than one TEC receiver station. Stations in the neighbor countries can also be considered for study. There is IGS station in Addis Ababa in Ethiopia and another one in Uganda. Such stations can be considered for study.

References

1. Baumjohann, W. and Rudolf, A. T., (1997). *"Basic Space Plasma Physics"*. Imperial College Press, London.

2. Moldwin, M. (2008). *An Introduction to Space Weather*. Cambridge University Press, 71-73

3. Kunitsyn, V. E., Tereshchenko, E. D., (2003). *"Ionosperic Tomography"*. Springer-Verlag Berlin. Lecture Notes Phys. 699, 143-164.

4. Zou, Y. and Wang, D. (2009). *A study of GPS ionospheric scintillations observed at Guilin*. Journal of Atmospheric and Solar—Terrestrial Physics 71 1948—1958.

5. Thompson, A. R., Moran, J. M. and Swenson G. W. Jr, (2004). *Interferometry and Sylnthesis in Radio Astronomy, Second Edition*. Wiley-Vch Verlag Gmbh & Co. Kgaa,576

6. Mala, S. Bagiya, Joshi H. P. , Iyer K. N., Aggarwal M., Ravindran S., and Pathan B. M. (2009). *TEC variations during low solar activity period (2005–2007) near the Equatorial Ionospheric Anomaly Crest region in India*. Annales Geophysicae, 27, 1047–1057.

7. Klobuchar J. A., Doherty, P. H., El-Arini, M. B., (1995). *"Potential Ionospheric Limitations on GPS Wide – Area Augmentation System (WAAS)"*. Navigation Journal of the Institute of Navigation, Vol. 42, No. 2.

8. Whitten, R. C. and Poppaff, I. G., (1971). *"Fundamentals of Aeronomy"*. New York: J. Wiley and Sons. Inc.

9. Liu, J. Y., Chen, C. H., Chen, Y. I., Yang, W. H., Oyama, K. I. and Kuo, K. W., (2010). *"A statistical study of ionospheric earthquake precursors monitored by using equatorial ionization anomaly of GPS TEC in Taiwan during 2001–2007"*. Journal of Asian Earth Sciences 39 76–80.

10. Suzuki S., Shiokawa K., Otsuka Y., Ogawa T., Kubota M., Tsutsumi M., Nakamura T., and Fritts D. C. (2007). *Gravity wave momentum flux in the upper mesosphere derived from OH airglow imaging measurements*. Earth Planets Space, 59, 421–428,
11. Stockwell, R. G. and Lowe, R. P. (2001). *Air imaging of gravity waves: Result from small network of OH nightglow scanning imagers*. Journal of Geophysical Research, Vol. 106, No D15, Pages 17,185-17,203.
12. Hunsucker, R. D. and Hargreaves, J. K., (2003). *The high-latitude ionosphere and its effects on radio propagation.* Cambridge University Press, ISBN-13 978-0-511-06742-6 eBook (EBL), page 181,203.
13. Klobuchar, J. (1986). *Design and characteristics of the GPS ionospheric time-delay algorithm for single frequency users, in: Proceedings of PLANS'86 – Position Location and Navigation Symposium*, Las Vegas, Nevada, p. 280–286, 4–7.
14. Rama Rao P. V. S., Gopi Krishna S., Niranjan K., and Prasad D. S. V. V. D. (2006). *Temporal and spatial variations in TEC using simultaneous measurements from the Indian GPS network of receivers during the low solar activity period of 2004–2005.* Annales Geophysicae 24, 3279–3292.
15. Sethi, N. K., Dabas, R. S., Singh, L., Vohra, V. K., Veenadhari, B. and Garg, S. C., (2003). *"Results of foF2 and Ne-h Profiles at Low Latitude Using Recent Digital Ionosonde Observations and Their Comparison with IRI-2000"*. Journal of Atmospheric and Solar-Terrestrial Physics 65 (6), 749–755.
16. Wright, J. W., (1962). *"Dependence of the Ionospheric F Region on the Solar Cycle"*. Nature 194, 461 - 462; doi:10.1038/194461a0.
17. Chapman S. (1956). *The electrical conductivity of the ionosphere: a Review,* Geophysical Institute—University of Alaska, High Altitude observatory—Boulder, Colorado

18. Radicella, S. M., Nava B., Pulinets, S. and Depuev, V., (2001). *"Modelling bottom and topside electron density and TEC with profile data from topside ionograms"*. Advances in Space Research, V. 27, pp. 31—34,.

19. Forte, B., Radicella, S. M. and Ezquer, R. G., (June/August 2002). *"A different approach to the analysis of GPS scintillation data"*. Annals of Geophysics, VOL. 45, N. 3/4, 551-561

20. Buonsanto M. J., (1999). *Ionospheric Storms- A Review*. Space Science Reviews, 88. Massachusetts Institute Of Technology, Haystack Observatory, Westford, Ma 01886, U. S. A., 563-601.

21. Basu, Su., Basu, S., Huba, J., Krall, J., McDonald, S. E., Makela, J. J., Miller, E. S., Ray, S. and Groves, K., (2009). *"Day-to-day variability of the equatorial ionization anomaly and scintillations at dusk observed by GUVI and modeling by SAMI3"*. Journal of Geophysical Research, Vol. 114, A04302, doi: 10.1029/2008JA013899, 1-6.

22. Zain, A. F. M. and Abdullah, M., (1999). *"Initial results of total electron content measurements over Arau, Malaysia"*. Proc. 4th IEEE Malaysia International Conference on Communications Vol. 1, 440- 443.

23. Kappenman, J. G. (2003). *Storm sudden commencement events and the associated geomagnetically induced current risks to ground-based systems at low-latitude and mid-latitude locations*. Space Weather, 1(3), 1016, doi:10.1029/2003SW000009.

24. http://igscb.jpl.nasa.gov/mail/igsmail/2001/msg00146.html accessed on 7th March 2013.

25. http://www.ngs.noaa.gov/IGSWorkshop2008/docs/net-soehne.pdf accessed on 15th March 2013.

26. Davies, K., (1990). *Ionospheric Radio*. IEE Electromagnetic waves series, 31, ISBN 086341186X

27. Titheridge, J. E., (1985), *Ionogram Analysis : Least squares fitting of a chapman layer peak*. Radio Science, 20, No: 2, Pp: 247-256.

28. Batlló, J. and Altadill, D., *"The Ebre observatory – Its path to ionospheric research"*. Observatori de l'Ebre, Universitat Ramon Llull, CSIC, Carretera de l'Observatori 8, E-43520 Roquetes, Spain. http://digital.csic.es/bitstream/10261/4502/3/Batllo_EbreObservatory.pdf, 15th April 2012.
29. Rodés, L., (1927). *"Some new remarks on the cause and propagation of magnetic storms"*. J. Terr. Magnet. Atmos. Electr. 32, pp. 127–131. http://nopr.niscair.res.in/handle/123456789/11195, 15th April, 2012.
30. Hanson, W. B. and Moffet, R. J., (1966). *"Ionization transport effects in the equatorial F-region"*. Journal of Geophysical Research, 71, 5559,.
31. Ossakow, S. L., (1981). *"Spread-F theories: A review"*. Journal of Atmospheric and Solar-Terrestrial Physics, 43, 437-452, doi:10.1016/0021-9169(81)90107-0.
32. Tsunoda, R. T., (2005). *"On the enigma of the day-to-day variability in equatorial spread F"*. Geophysics Research letter, 32, L08103, doi:10.1029/2005GL022512.
33. Basu, S. and Costa, E., (2002). *"A radio wave scattering algorithm and irregularity model for scintillation predictions"*. Radio Science, Vol. 37, 1046, 14 Pp., Doi:10.1029/2001rs002498.
34. McDonald, S. E., Dymond, K. F. and Summers, M. E., (2008). *"Hemispheric asymmetries in the longitudinal structure of the low-latitude nighttime ionosphere"*. Journal of Geophysical Research, 113, A08308, doi:10.1029/2007JA012876.
35. Chauhan, V., Singh, O. P. and Singh, B., (2011). "D*iurnal and seasonal variation of GPS_TEC during a low solar activity period as observed at a low latitude station, Agra"*. Indian Journal of Radio and Space Physics Vol. 40, pp. 26-36.
36. Olwendo J.O., Cilliers P.J., Baki P. and Mito C. *Using GPS-SCINDA observations to study the correlation between scintillation, total electron content*

enhancement and depletions over the Kenyan region. Advances in Space Research 49 (2012) 1363–1372

37. Bagiya M. S., Joshi H. P., Iyer K. N., Aggarwal M., Ravindran S., and Pathan B. (2009). M. *TEC variations during low solar activity period (2005–2007) near the Equatorial Ionospheric Anomaly Crest region in India.* Annales Geophysicae 27, 1047–1057.

38. Bolaji, O. S., Adeniyi, J. O., Radicella, S. M., and Doherty, P. H., (2012). *Variability of total electron content over an equatorial West African station during low solar activity.* Radio Science, Vol. 47, Rs1001, Doi:10.1029/2011rs004812.

39. Namba, S. and K.-I. Maeda (1939). *Radio Wave Propagation*, 86 pp., Corona, Tokyo.

40. Appleton, E. V. (1946). *Two anomalies in the ionosphere.* Nature, 157, 691.

41. Duncan, R. A. (1960). *The equatorial F region of the ionosphere.* J. Atmos. Terr. Phys., 18, 89.

42. Data - GNSS & Archive Glossary. http://facility.unavco.org/data/glossary.html, 7th September 2012.

43. Kenya Literature Bureau (2005). *Secondary Mathematics Students Book Four.* Kenya Literature Bureau, Pages 46 and 47.

44. Lin Chien-Hung, Liu Jann-Yenq, Tsai Ho-Fang, and Cheng Chio-Zong (2007). *Variations in the equatorial ionization anomaly peaks in the Western Pacific region during the geomagnetic storms of April 6 and July 15, 2000.* Earth Planets Space, 59, 401–405.

45. jZip A Free WinZip Alternative, http://www.jzip.com/ 24th January 2013.

46. World Data Center for Geomagnetism, Kyoto Operated By Data Analysis Center for Geomagnetism and Space Magnetism Graduate School of Science,

Kyoto University -http://wdc.kugi.kyoto-u.ac.jp/cgi-bin/dstae-cgi?SCent=20&STens=0&SYear=0&SMonth=01&ECent=20&ETens=0&EYear=0&EMonth=12&Output=PLOT&Image+Type=GIF&COLOR=COLOR&AE+Sensitivity=0&Dst+Sensitivity=0&Out+format=WDC&Email=gondede%40ictp.it 9th May 2012

47. SIDC—Solar Influence Data Analysis Centre- http://www.sidc.be/ 1st April 2012
48. Real Time Ionospheric Scintillation – BRASIL Current GPS S4 Data Display - INPE - Sao Luis -MA Cascade – Station http://www.inpe.br/scintec/status?id=slz, 24th January 2012.